Chapter 7
Laser Surface Modification for Protection Against Wear

S.V. Joshi and Manish Roy

7.1 Introduction

With the advent of laser technology during the past few decades, surface modification using lasers has been used extensively. It was way back in the 1960s when Maiman [1] first invented a working ruby laser. This was followed by the diode laser proposed by Basov [2]. In 1962, diode laser was demonstrated independently by Hall et al. [3] at General Electric, Nathan et al. [4] at IBM and by Quist et al. [5] at MITs Lincoln Laboratory. The first CO_2 laser was invented by C.K.N. Patel soon thereafter in 1964 while working in Bell Labs [6]. In the same year Nd–YAG laser was also invented in Bell Labs. Ewing and Brau [7] came up with the excimer laser in 1974 in Avco Everett Laboratory. A free electron laser was first demonstrated by Madley's group at Stanford University. As a result of above developments, today optical energy is available in an easily controllable form and has therefore been gainfully initialized for various materials processing operations. The mastery gained over the use of laser initially as a tool for routine operations such as cutting drilling and welding has now enabled realisation of various surface modification approaches based on high power lasers.

Although widely perceived as being expensive, the laser based techniques offer several distinct advantages over other conventional surface modification processes. All variants of laser surface modification are characterised by very fast heating and cooling rates resulting in a rapidly solidified layer, in which both the microstructure and the distribution of the alloying elements could be tailored as required by

S.V. Joshi (✉)
International Advanced Research Center for Powder Metallurgy and New Materials, Balapur, Hyderabad 500005, Andhra Pradesh, India
e-mail: SVjoshi.uoh@gmail.com

M. Roy
Defence Metallurgical Research Laboratory, Kanchanbagh, Hyderabad 500058, Andhra Pradesh, India

M. Roy (ed.), *Surface Engineering for Enhanced Performance against Wear*,
DOI 10.1007/978-3-7091-0101-8_7,

suitably controlling the operating parameters. The metastable and non-equilibrium phases that can form as a consequence of rapid quenching, offer the possibility to develop layers with novel microstructures and properties superior to those of traditional processes. Laser energy is highly directional and it can be controlled precisely and with the use of appropriate optics, the beam can also be shaped into a spot, line or area beam as required. Due to directionality of laser light, it is possible to utilise a laser beam to treat locations that are difficult to approach. Laser light can also be of very short duration which allows deposition of large amount of energy into a very narrow region. Moreover, laser-based processes are chemically clean, extremely environment friendly and generally do not require any post-processing treatment. The fact that the process is very and can be automated easily is a significant-added benefit. Laser surface-modified components also have minimum risk of distortion as the heat input is highly localised and the part being treated serves as a substantially large heat sink to prevent overheating of the bulk component. With the advent of high power diode laser, the concerns regarding maintenance have also been largely alleviated to make laser considerably user friendly.

The above unique advantages offered by a laser make it an unparallel tool for surface modification. Surface engineering is a subject of growing industrial interest as it allows fabrication of improved components with an ideal combination of surface and bulk properties to enhance performance, extend life, improve aesthetics, etc. Realising its relevance in the current competitive era, engineering industries have become increasingly receptive to improved, sophisticated and advanced surface modification techniques for development of high performance coatings. Growing awareness of laser surface modification and its immense potential have made laser surface processing an integral part of modern technology and industry. In view of the above, this chapter is intended to provide an overview of laser surface modification specifically for tribological applications.

7.2 Laser Surface Modification Processes

7.2.1 Process Fundamentals

During laser surface modification, several process parameters significantly influence the microstructure and mechanical properties of the modified layer. The prominent among them are traverse speed, power density, extent of overlap, etc. As the power density is influenced by beam spot area, the beam diameter/shape is important. The nature of surface treated in respect of absorbance of the incident laser energy is also a determining factor. Apart from the above generic factors, the powder feed rate (or amount of powder preplaced) are important too, in case of laser alloying. Additionally changes in these parameters result in change in depth, width and microstructure of the modified region as well as its functional properties. An increase in beam power is found to increase the width and depth of the modified layer [8, 9]. Higher scan speed and lower laser power lead to faster cooling rates

giving rise to a finer microstructure. For example, a higher scan speed has been reported to result in changes from dendritic microstructure to cellular microstructure during laser carburizing of Ti–6Al–4V [10]. The laser power density (q) for a continuous wave laser and a pulsed laser is given by following equation:

$$q = \frac{P}{A} \tag{7.1}$$

and

$$q = \frac{P}{A\tau} \tag{7.2}$$

where P is the power of the laser, A is the area of the beam and τ is the duration of the pulse of the laser. The radius (r_s) of the beam spot is related to the wavelength (λ), beam quality factor, K, the focus distance of the lens (f) and the beam diameter (D) by the following expression:

$$r_s = \frac{2\lambda}{\pi}\frac{f}{D}\frac{1}{K} \tag{7.3}$$

The type of laser employed plays a crucial role in governing the nature of the modified layer. It is widely acknowledged that if the surface is to be modified by co-deposition of an alloying element or by cladding, a continuous laser is better suited than a pulsed laser [11]. On the contrary, it has been reported that, for laser gas nitriding of Ti–6Al–4V, a pulsed laser provides a better surface finish than that achieved using a continuous laser [12]. During co-deposition by laser cladding, the clad layer thickness increases with laser power for a given traverse speed and clad thickness [13], whereas the clad layer thickness decreases with traverse speed when other process parameters are kept constant [14]. There is clear evidence that the clad layer thickness increases monotonically with powder feed rate [13]. The extent of overlapping and rescanning are two key parameters which govern the nature of modified layer. Rescanning with a defocused beam during laser carburizing improves the surface roughness and homogeneity of the modified layer [12].

The heat input is essentially governed by the ratio of laser power to traverse speed. A key parameter known as the side bead angle is particularly important in multipass cladding. A side bead angle greater than 120° generally results in good integrity in the overlap zone between consecutive passes. Angles lower than 120° lead to increase impurity trapping and less fusion in the overlapped region. The side bead angle increases rapidly with powder depth in case of preplaced powder and powder feed rate in case of dynamic powder feeding. This parameter is not strongly affected by either laser power or travel speed. Thermophysical properties such as relative melting point, vapour pressure of the elements are known to play a crucial role. In case of high vapour pressure alloying species high evaporation loss is noted [15, 16]. Alloying low melting point element with a high melting point substrate is

fraught with difficulties relating to bobble formation and entrapment in the resolidified near surface region [17]. Liquid state miscibility is another governing factor, for example, it is much easier to alloy in systems like Pd–Ni but difficult to alloy in system like Ag–Ni.

Dilution, another important parameter in laser surface modification, is defined as the percentage of the total volume of the surface-modified layer contributed by melting of the substrate. It is usually estimated by area measurement of the cross section and is given as ratio of the area of the melted substrate to the sum of the area of the deposit and the area of the melted substrate. It can also be calculated by measuring the composition of the as processed surface layer as

$$\text{dilution} = \frac{\rho_{\mathrm{A}}(\%N_{\mathrm{A+S}} - \%N_{\mathrm{A}})}{\rho_{\mathrm{S}}(\%N_{\mathrm{S}} - \%N_{\mathrm{A+S}}) + \rho_{\mathrm{A}}(\%N_{\mathrm{A+S}} - \%N_{\mathrm{A}})} \tag{7.4}$$

where ρ_{A} is the density of the alloying material, ρ_{S} is the density of the substrate, N_{A} is the weight percent of the element N in alloying material, N_{S} is the weight percent of the element N in the substrate and $N_{\mathrm{A+S}}$ is the weight percent of the element N in total surface layer. In order to assess the influence of process parameters on dilution, it is imperative to define the parameter specific energy. Specific energy is defined as the ratio of the laser power to the product of the beam width and travel speed. Dilution has been widely reported to increase with specific energy. As expected, the increase in dilution with specific energy is much more rapid in cases where surface treatment is carried out with powder preplaced to a shallow depth as compared to deeper powder layer depth. For a given powder layer depth and specific energy, the dilution increases with increasing power density.

7.2.2 Process Classifications

Laser surface modification encompasses a large variety of processing techniques. If laser surface modification is carried out without addition of any consumables, the process can be designated as laser transformation hardening and/or laser diffusion homogenization. If the modification results in superficial melting of the substrate followed by rapid solidification, it may be called laser glazing [18]. When extraneous materials are added to the substrate surface during laser processing, it can be classified as laser surface alloying or laser cladding [19–22]. In terms of processing, alloying and cladding are very similar and the differentiation between the two is largely based on the extent of dilution—somewhat arbitrarily the process is termed as cladding if the dilution exceeds 10 %. Laser surface modification can also be classified under different heads on the basis of number of steps involved, namely single-step laser deposition process and two-step laser deposition process. The one-step laser deposition technique consists of dynamically injecting the powder into the laser beam–substrate interaction zone where the powder is heated (melted) and

subsequently deposited on the substrate. The most recent industrial application of one-step laser deposition is rapid prototyping, which enables direct production of components having complicated three-dimensional shapes. Two-step laser deposition consists of laser treatment of a pre-deposited coating. The pre-deposition can be carried out by any of the numerous thin and thick coating techniques available or, in its simplest form, by merely brushing on the alloying/cladding material mixed with a suitable binder. Popular among the pre-deposition processes is thermal spraying, which is often simplest to apply a reasonably thick uniform layer of the alloying/cladding material.

7.2.2.1 Laser Heat Treatment

Laser heat treatment is a process which uses the rapid heating and cooling rates produced on the metal surface exposed to scanning laser beams and offers several advantages over conventional surface hardening processes. Laser heat treatment processes can broadly be classified into laser transformation hardening and laser remelting. Transformation hardening is more commonly applied laser heat treatment and is induced by heating a material above a critical temperature and then rapidly quenching it rather than allowing equilibrium phases to form. Steels and cast irons are good candidate materials for laser transformation hardening. On the other hand, laser remelting operations involve melting of the surface and are carried out at lower scan speeds or higher power levels. Although a relatively low power density is utilised for both forms of heat treatment, the cross-sectional area of the beam used to scan the part being heat treated is normally much larger than the focused beam used for welding and cutting to enable large area processing at practically meaningful speeds. Therefore higher beam power is required for laser heat treatment. A schematic representation of laser transformation hardening process is provided in Fig. 7.1. During transformation hardening, the laser beam is defocused or oscillated to cover the desired area with a power density of 10^3–10^4 W/mm^2 and a relative motion between the work piece and the beam of 5–50 mm/s. An ideal power distribution is one which gives a uniform temperature over the area to be treated. It is relevant to note that a laser beam is extremely flexible and it offers unparallel versatility to enable time share and power share as well as single focus, dual focus and defocused configurations. The flexibility is illustrated by schematics in Fig. 7.2 and further reinforced by ability to shape beams through use of appropriate optics. Typical microstructures of several varieties of steels with varying carbon content after laser transformation hardening are provided in Fig. 7.3. Very fine microstructure due to transformation hardening is evident. The advantages and disadvantages of laser transformation hardening compared with other hardening processes such as induction hardening and flame hardening is summarised in Table 7.1.

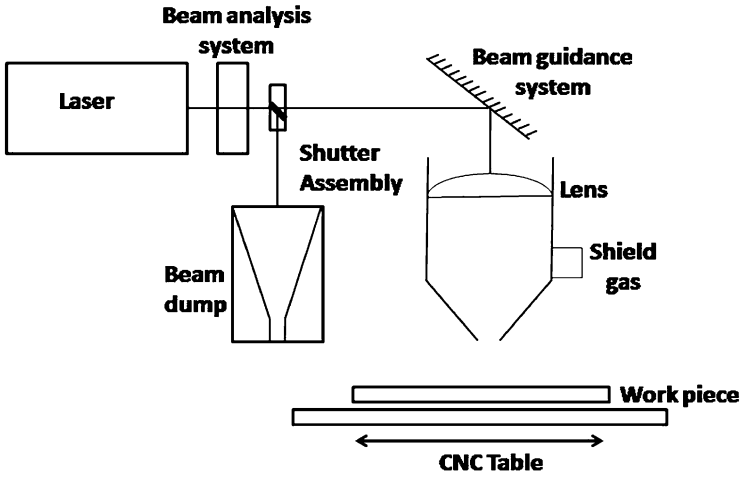

Fig. 7.1 Schematic representation of laser transformation hardening system

7.2.2.2 Laser Glazing

Laser glazing involves surface melting followed by rapid self-quenching resulting in a fine or amorphous microstructure. Experimental arrangement for laser glazing is similar to laser transformation hardening. The surface to be melted is shrouded by an inert gas. In this process, the most important variables are reflectivity of glazed surface, shape of the beam, shrouding of the melt pool, apart from the laser power and scan speed. It is difficult to control the reflectivity of a molten surface. As the material becomes hot, reflectivity decreases due to increased concentration of phonons. Figure 7.4 shows typical microstructures of as-plasma-sprayed and laser-glazed WC–Co coatings at two different scan speeds. Laser glazing can potentially reduce the porosities of the coated layer and also refines the microstructures to achieve improved mechanical properties. The extent of refinement and property enhancement is however dependent on the laser power and scan speed.

7.2.2.3 Laser Surface Alloying

Laser surface alloying is a process in which a component of the alloy is injected into the molten pool on the substrate during processing. Although alloying element is generally added in powder or wire form, introduction in the gaseous form is also possible. Alloying requires a greater laser power density, as substantial energy is expended to create a melt pool on the substrate and often also melt the injected powder on the substrate surface. The alloying process enables formation of metallic and ceramic alloys, such as nitrides or borides. The process starts with melting of a substrate by laser irradiation. On the surface of the melt pool, there is a temperature

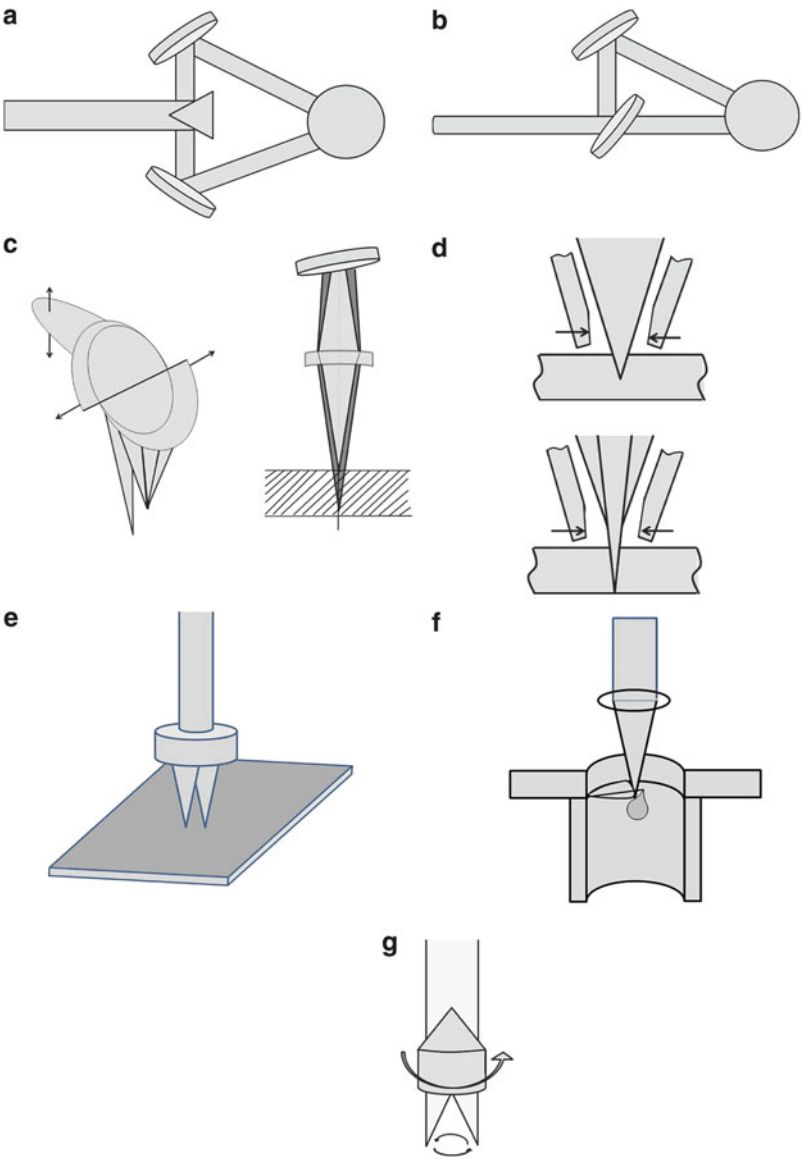

Fig. 7.2 Various optics options illustrating the flexibility of a laser beam for materials processing

distribution, which results in the differential surface tension distribution. The shear stress, which is equal to the gradient in surface tension, pulls the material from the centre and causes convection currents within the melt pool. In case of the injection of solid particles into the melt, the convection permits good mixing with the substrate material within the alloyed layer. The particles are sometimes also melted

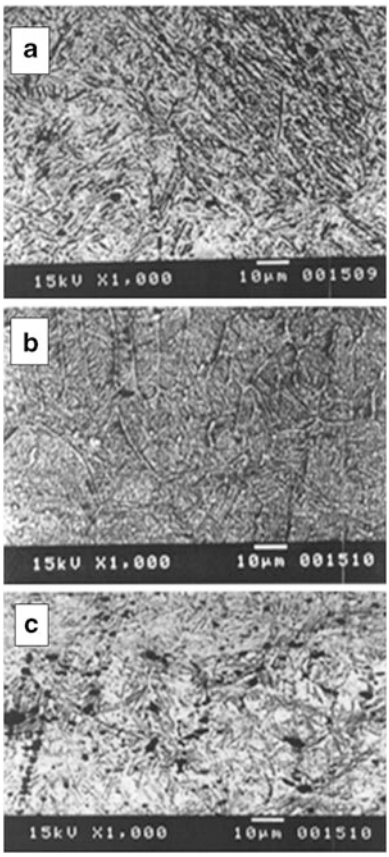

Fig. 7.3 SEM images of several varieties of steels after laser transformation hardening

Table 7.1 The advantages and disadvantages of laser transformation hardening with other hardening processes

Characteristics	Laser hardening	Induction hardening	Flame hardening
Distortion	Very low	High	Very high
Quenching requirement	No	Yes	Yes
Process rate	High	High	Low
Case controllability	Easily controllable	Controllable	Non controllable
Post processing	Not required	Required	Required
Thickness limitation	No	Depends on job	Yes
Equipment cost	Very high	High	Very low
Process flexibility	High	Low	Very low
Special requirement	Absorbent coating	Depends on job	Not required
Automation	Possible	Not possible	Not possible
Selective treatment	Possible	Not possible	Not possible

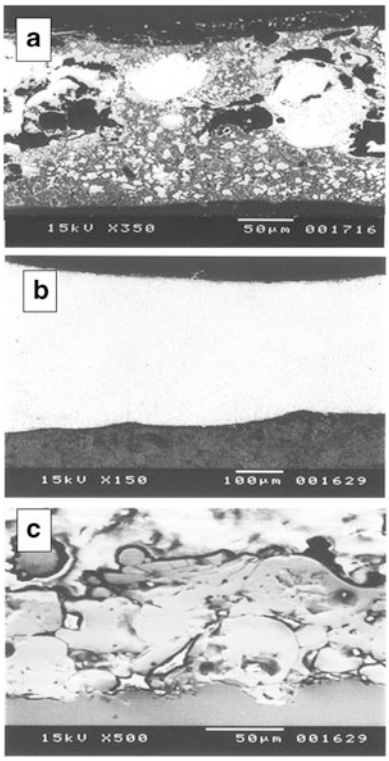

Fig. 7.4 SEM images of as-plasma-sprayed and laser-glazed WC–Co coatings

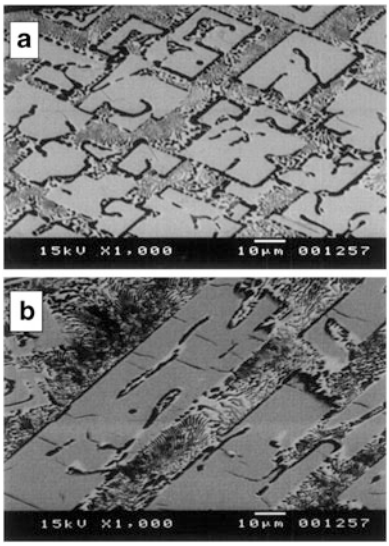

Fig. 7.5 SEM images showing the microstructure obtained by laser boronising of steel

and reaction with the substrate can take place. The reaction slows down and stops soon after the laser beam moves to the next position. The subsequent rapid cooling of the melt makes it possible to form metastable or high-temperature phases as the product of the reaction. However, the cooling rate can also be slowed by lowering of laser beam speed over the substrate. The microstructure of the layer resulting from laser alloying of the steel substrate with iron boride is shown in Fig. 7.5. Through such alloying, the surface properties of the substrate can virtually be tailored (for wear resistance, corrosion resistance, etc.) to meet the requirements dictated by any given application.

7.2.2.4 Laser Cladding

Laser cladding can be defined as addition of extraneous material with limited substrate melting resulting in development of a metallurgically bonded coating on the substrate to yield a surface with completely different composition and structure compared to the base material. In contrast, laser surface alloying involves relatively lower amount of consumable material addition giving rise to a compositionally modified surface layer. As previously mentioned, laser cladding is differentiated from laser surface alloying depending on the extent of dilution of the surface layer from the base material. If the surface layer is diluted to an extent less than 10 %, it is called laser surface alloying. The manner in which the extraneous material is added in the interaction zone often varies in different processes. The coating materials are commonly added in the form of powder or wire in case of both laser alloying and laser cladding.

The objective of laser cladding is to deposit a completely different layer on the substrate with a sound interfacial bond without any dilution. Laser cladding can be done either with preplaced powder (two-step laser processing) or with blown powder as shown in Fig. 7.6 or by wire feeding. The physics of the cladding process using coaxial injection of powder has been analysed in reported literature [23–25]. It was found that there is a certain minimum power necessary to produce the coating. This power corresponds to the beginning of substrate melting. The velocity of the injected powder particles was determined using laser Doppler velocimetry (LDV), and values of 1–2.5 m/s has been reported. The laser power density necessary for in-flight melting of the particles has been estimated and theoretically found to be in the range of $q = 5$–7 kW/cm^2 in the case of Stellite 6 alloy. The cladding of the same material was analysed theoretically [24] for a powder injection system and it has been found that the powder efficiency can be as high as 69 % for a linearly polarised CO_2 laser beam at high angles of incidence (the angle between the normal to a molten pool and the laser beam axis). Lin [26] and Hayhurst et al. [27] found that the powder stream can be mildly focussed with a coaxial nozzle. Lin used a circumferential powder feeder and obtained best focus when the central nozzle was slightly proud of the outer nozzle to encourage some couette flow of the powder. Hayhurst et al. [27] employed four independent powder injection streams 90° apart, which on colliding merge into a single central stream. One variation of

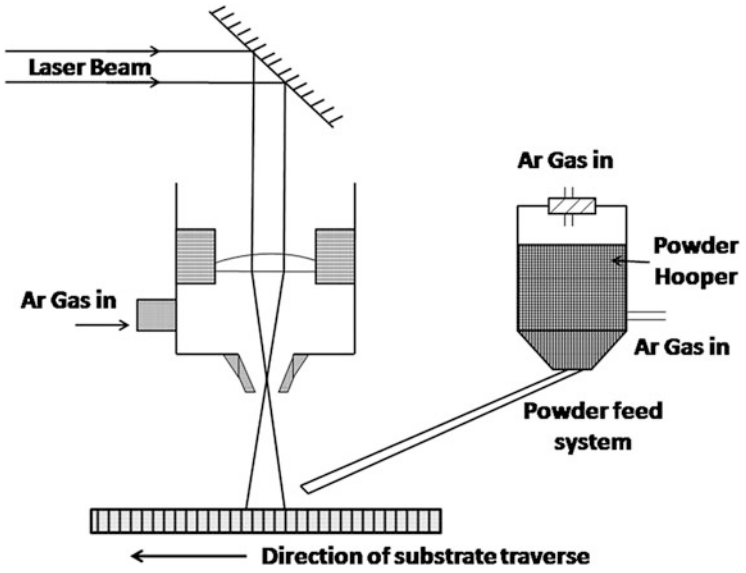

Fig. 7.6 Schematic representation of laser cladding by blown powder

laser cladding is known as bi-thermal laser cladding [28] in which powder is fed into the focal spot of the laser beam and melts instantaneously. The molten powders are then allowed to impact the substrate which is situated at lower power density. Employing this technique it was possible to coat chromium on aluminium. Such coating is rather difficult by conventional process.

7.2.2.5 Laser Composite Processing

Laser hard phase dispersion is a coating process that consists of injecting hard second-phase particles into a melted substrate. These particles remain solid during laser processing. After solidification, the hard particles are dispersed in a matrix of the substrate material throughout the modified layer. This process, which produces metal matrix composites (MMCs), was initiated in the 1970s [29] and is in many ways similar to alloying. As there is convection in a molten pool, the reinforcement powder injection angle and spot need to be carefully optimised. Kloosterman and De Hosson [30] found that the powder injection spot should be centred inside a laser beam. Any other position produces a less homogenous dispersion of particles in the modified layer. The depth of particle penetration depends on the injection velocity, which is determined, in turn, by the carrier gas flow. An increase in powder feed rate can transform a hard phase dispersion process into a cladding process if correspondingly higher power to ensure complete melting is employed. To achieve a condition wherein the substrate melts, but the hard particles remain solid, the temperature of the melt must be well below the melting point of the hard phase. If

this is not possible, one can increase the traverse speed to limit the time of particle dissolution in the melt. However, rapid solidification of the melting pool, which includes particles of hard phase, can generate residual stresses that can lead to cracking of the coating. Cracks can be avoided by preheating the substrate prior to coating, although such heating essentially makes the process a two-step one. In order to achieve a good surface-modified layer, the particles must be wetted by the substrate material and should also be strongly bound to it. The particles should not dissolve in the molten pool during processing. Carbides are most frequently used as the hard phase. Injection of B_4C in a steel matrix has also been shown to produce Fe_3B and $Fe_{23}B_6$ [31], while injection of SiC in an aluminium matrix resulted in $AlSiC_4$ as a solution product [32].

7.2.3 Process Governing Equations

7.2.3.1 Heat Flow Equations

The governing differential equation for conduction of heat in stationary medium when there is no heat loss due to convection or radiation is

$$\Delta^2 T = \frac{1}{\alpha}\frac{\partial T}{\partial t} \tag{7.5}$$

During transformation hardening using continuous laser, the temperature at any point of hardening can be derived using the moving point source by Ashby and Easterling [33]. In this model, it is assumed that the work piece is semi-infinite, homogeneous, isotropic having constant thermal properties. This model does not account for heat loss due to transformation, radiation and convection. According to this model, temperature at any point beneath the heat source is given by

$$T - T_o = \frac{Aq/v}{2\pi k[t(t+t_o)]^{1/2}} \exp\left\{-\frac{1}{4\alpha}\left[\frac{(z+z_o)^2}{t} + \frac{y^2}{t+t_o}\right]\right\} \tag{7.6}$$

where T_o is the initial temperature, A is the absorptivity at the sample surface, q is the input energy, k is the thermal conductivity (W/m/K), v is the scan speed (m/s), z is depth below the surface (m), z_o is a length constant, y is distance in Y-direction, t is time (s), t_o is the time at the start of power (s) and α is thermal diffusivity (m^2/s). This model can be used conveniently for explaining transformation laser surface hardening.

The moving Gaussian surface heat source model was first solved by Cline and Anthony [34] and Devis et al. [35]. Employing this model it is possible to derive an expression for the depth of hardness assuming constant thermal properties, no latent

heat effect and no surface heat loss by convection or radiation. Accordingly the depth of hardness can be obtained as

$$d = 0.76D \times \left[\frac{1}{(\alpha' C/q) + \pi^{1/4}(\alpha' C/q)^{1/2}} - \frac{1}{(\alpha' C/q_{\min}) + \pi^{1/4}(\alpha' C/q_{\min})^{1/2}}\left(\frac{q_{\min}}{q}\right)^3\right] \tag{7.7}$$

where $\alpha' = \frac{\rho u D C}{2k}$, $q = \left[\frac{2P(1-r_f)}{D\pi^{3/2}k(T_c - T_o)}\right]$, $q_{\min} = (0.40528 + 0.21586C)^{1/2}$

with $q_{\min}$ = the minimum absorbed power for which any hardening can occur and

$$C = C_\infty - 0.4646(C_\infty - C_0)(\alpha C_0)^{1/2} \tag{7.8}$$

The constants vary with materials and values determined employing this equation fits quite well with experiments [36].

7.2.3.2 Solidification Equations

Considering the mass balance on the solidification front, the gradient of the solute in the liquid at the solidification interface is obtained as

$$\left[\frac{dC_L}{dx}\right]_{x=0} = -\frac{R}{D_L}C_L^*(i-k) \tag{7.9}$$

Constitutional super cooling will be absent if the temperature gradient in the liquid at the interface (G) satisfies the condition

$$G \geq \left(\frac{dT_L}{dx}\right)_{x=0} \tag{7.10}$$

The value of this gradient can be obtained as

$$\left[\frac{dT_L}{dx}\right]_{x=0} = m_L\left[\frac{dC_L}{dx}\right]_{x=0} \tag{7.11}$$

where C_L is liquidus composition, x is the distance from the interface, T_L is the liquidus temperature in °C, R is the rate of solidification, D_L is diffusivity in m^2/s, C_L^* is the liquidus composition in equilibrium with solidus composition C_S^*, k is partition coefficient, m_L is the slope of the liquidus and G is thermal gradient in °C/m.

Combining Eqs. (7.9) and (7.11) and assuming $C_S^* = C_L^*$ at equilibrium, criterion for general constitutional supercooling is obtained as

$$\frac{G}{R} \geq -\frac{m_L C_S^* (1-k)}{k D_L} \tag{7.12}$$

When the ratio of G/R is very large, planar front solidification takes place. When this ratio is very small, regimes for 'absolute stability' comes into play.

Scales of solidification structures can be obtained by employing Fick's second law as

$$D_L \frac{\delta^2 C_L}{\delta y^2} = \frac{\delta C_L}{\delta t} \tag{7.13}$$

$$\frac{dC_L}{dt} = \left(\frac{dC_L}{dT}\right)\left(\frac{dT}{dx}\right)\left(\frac{dx}{dt}\right) = -\frac{GR}{m_L} \tag{7.14}$$

Substituting (dC_L/dt) from Eq. (7.14) and integrating across the cell width λ following expression is obtained:

$$\left[\frac{\delta C_L}{\delta y}\right]_{y=0} = -\frac{GR\lambda}{m_L D_L} \tag{7.15}$$

and

$$\Delta C_{L_{max}} = -\frac{GR\lambda^2}{2 m_L D_L} \tag{7.16}$$

Thus cell spacing is inversely related to the square root to the product of G and R or the cooling rate. Thus, higher the product of G and R, finer is the microstructure.

7.2.3.3 Fluid Flow Velocity in the Melt Pool

There are many forces those act in the melt pool. The largest among them is variation of surface tension due to steep thermal gradient. Anthony and Cline [34] have derived a simplified expression for fluid flow velocity driven by surface tension gradient during laser processing as

$$U_x(y,t) = \frac{1}{\eta}\frac{d\sigma}{dT}\Delta T\left[(D_u t)^{1/2} - y\right] \tag{7.17}$$

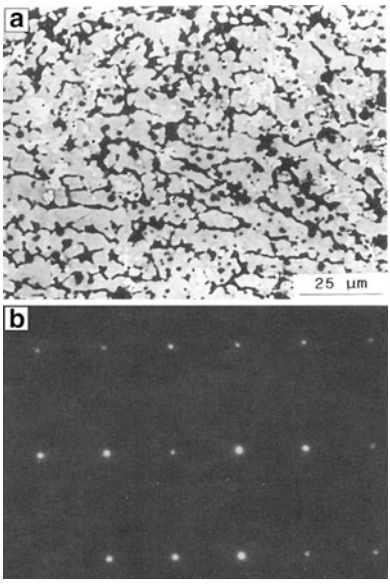

Fig. 7.7 Back scatter electron image of laser-Ti alloyed LM-9 with corresponding electron diffraction pattern [37]

Where $U_x(y,t)$ is the liquid velocity in the x direction at any given depth y and at any time t, η is the viscocity, $d\sigma/dT$ is temperature coefficient of the surface tension of the liquid and D_u is the diffusivity of the velocity profile.

7.3 Characterisation of Laser Surface-Modified Layer

7.3.1 The Microstructure

The microstructure of laser-treated surfaces is often of paramount interest and has, consequently, been very widely studied for all types of laser surface-modified layers. For example, Das et al. [37] characterised the microstructure of laser-glazed and laser surface Ti and Ni-alloyed aluminium alloy LM-9. The alloyed layer can be divided in two sub regions. The alloying element was mainly confined in the upper sub region while the lower sub region was laser melted but contained very little alloying element. Alloying resulted in segregation of alloying elements in the alloyed region. A typical SEM image of the Ti-alloyed regions is illustrated in Fig. 7.7 along with the corresponding electron diffraction pattern. Ni was found to be more severely segregated than Ti. As homogenization of alloying elements during laser surface alloying takes place by surface tension driven convection, such segregation was attributed to higher density of nickel compared to titanium.

Certain constituents have been reported to refine the microstructure in laser-alloyed layer. For instances, the addition of CeO_2 refine the microstructure in laser-remelted alloy spray coatings, decrease the dendrite arm spacing, strengthen and

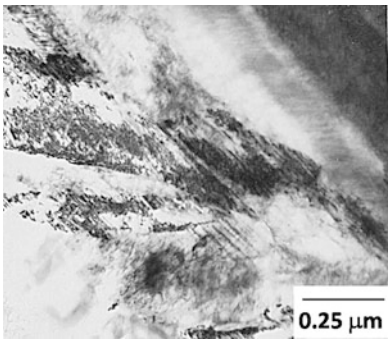

Fig. 7.8 TEM micrograph of the laser-remelted alloy spray coatings with CeO_2 having a martensitic structure [38]

purify the grain boundary, promote martensitic transformation and improve the morphology and distribution of eutectics and compounds. Martensitic as well as austenitic structure with lower density of dislocations can be found in laser-remelted alloy spray coatings with CeO_2. The martensitic structure has a high density of dislocation and fine twins. The morphology of martensitic structure includes lath-like, leaf-like, blocky and chrysanthemum-like shapes. Typical TEM micrographs of the laser-remelted alloy spray coatings with CeO_2 having martensitic structure is shown in Fig. 7.8 [38]. Figure 7.9 exhibits the eutectic martensite along with $M_{23}(CB)_6$ and the corresponding electron diffraction pattern.

Laser gas alloying is an important pathway for surface modification. Ti base alloys can be gas nitrided or gas carburised using a laser. Many fine TiN dendrites can be noted in the gas-nitrided laser surface-alloyed coatings. These dendrites are very hard and serve to enhance the wear resistance of the Ti–6Al–4V alloy. During laser surface melting under a nitrogen atmosphere, the nitrogen atoms dissolve in the high temperature Ti–6Al–4V melt, resulting in alloying of the melt-pool with nitrogen. After solidification of the alloyed melt bath, the wear-resistant 'in situ' composite reinforced by the as-solidified TiN dendrites is produced in the laser-melted surface layer. The laser beam scan rate has a significant influence on the microstructure of the laser surface-alloyed composite coatings. A lower beam scan rate results in a laser surface-alloyed composite coating having a higher volume fraction of TiN reinforcement due to the longer gaseous nitrogen and liquid interaction time. The average volume fraction of TiN dendrites decreases from approximately 62 to 40 % as the beam scan rate increases from 6 to 10 mm/s [39]. Similar observation is also reported by several other authors. With increasing scan speed, the cooling rate increases and the microstructure becomes finer as per Eq. (7.16). The influence of laser processing parameters on the microstructure is significant as illustrated in the work of Roy et al. [9]. Figure 7.10a, b shows the effect of scan power on the dendritic microstructure near the surface of the alloyed region obtained by laser nitriding commercially pure Ti. The dendritic structure is coarser for the melt pool obtained at higher power (2.1 KW) than the melt pool obtained at lower power (1.5 KW). It is also seen that the dendrites grow from the surface of the pool to the centre prior to the solidification of the centre. This indicates that the surface has solidified prior to the centre of the pool. Otherwise,

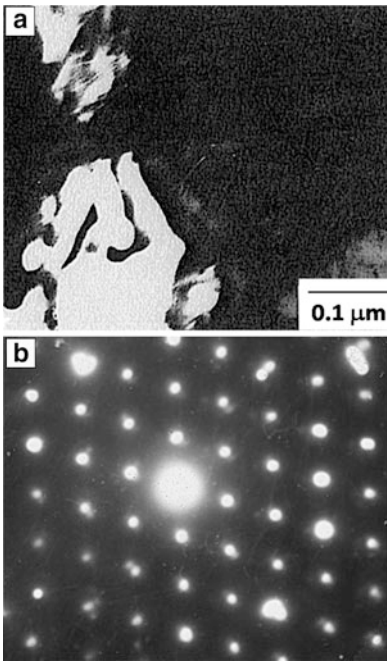

Fig. 7.9 Eutectic martensite along with $M_{23}(CB)_6$ and the corresponding electron diffraction pattern of the laser-remelted alloy spray coatings with CeO_2 [38]

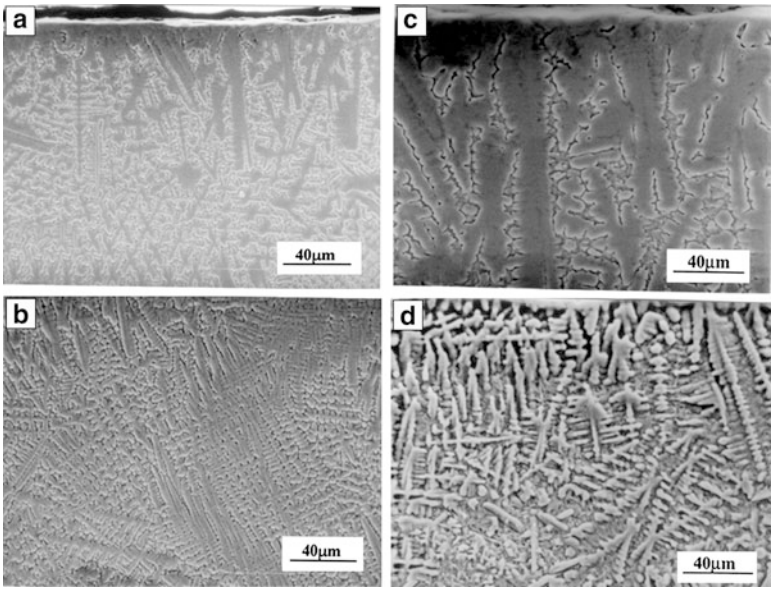

Fig. 7.10 Influence of laser processing conditions on the dendritic microstructure of Ti alloy [39]

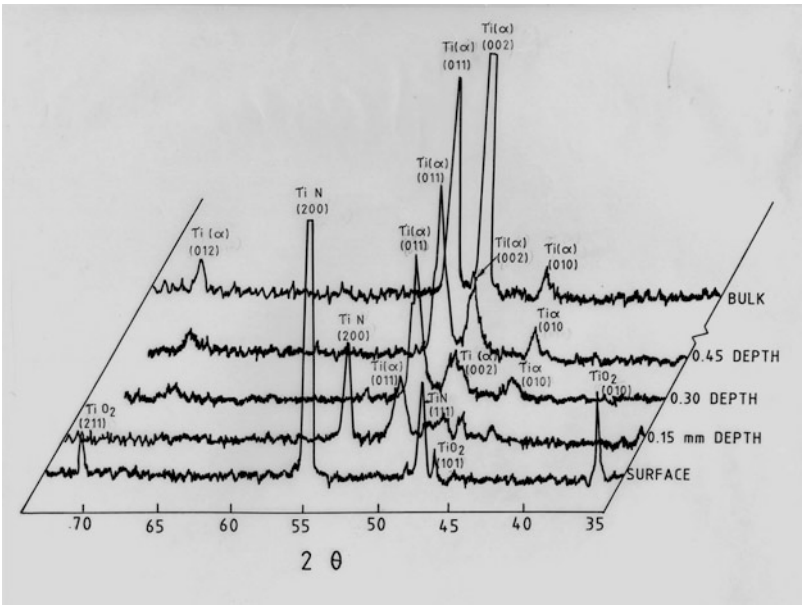

Fig. 7.11 Typical XRD patterns obtained at different depths in case of laser gas-nitrided Ti alloy [39]

in the alloyed melt pool, solidification starts at the surface and at the interface between the melted layer and unmelted substrate nearly at the same time. Such behaviour can be attributed to the formation of TiN layer near the surface of the melt pool. The temperature of the surface reaches below the melting point of high melting TiN phase almost at the same time as that of the region near the interface having low melting Ti (α). It can also be seen that the dendritic structure becomes finer with increasing laser scan speed as evident in Fig. 7.10c, d. This example is pertinent to note while investigating microstructure in laser-alloyed layer.

The X-ray diffraction technique is an important method to identify the phases present in laser-modified layers. A typical XRD pattern obtained from a laser gas-nitrided Ti alloy is shown in Fig. 7.11 [39]. Presence of hexagonal Ti and bcc TiN can be identified. It also indicates that, as one proceeds from the surface to the interior, the amount of TiN phase decreases and that of Ti (α) phase increases. Such composition gradient is often noted in laser-alloyed layer. The XRD pattern also reflects the changes in phase constitution as well as in the changes of quantity of various phases in the laser-modified layer on changing of processing conditions. The influence of laser beam scan speed on the XRD pattern is demonstrated by Staia et al. [40], who modified the surface of an A-356 alloy with a powder of 96 % WC, 2 % Ti and 2 % Mg in a two-step process with the help of a laser. The X-ray diffraction patterns obtained for the samples laser treated at different traverse velocities are represented in Fig. 7.12. Different carbides such as WC, W_2C and WC_x could be identified. The presence of small amount of WC_x can probably be

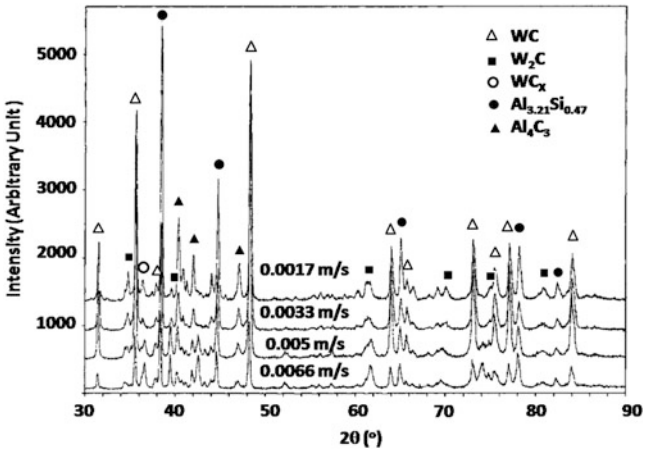

Fig. 7.12 X-ray diffraction patterns obtained for samples laser treated at different traverse velocities [40]

produced by partial dissolution of WC in the molten pool during laser processing and its subsequent solidification. Decarburisation of WC to W_2C is also a distinct possibility and widely reported. Decarburisation is accompanied by liberation of carbon which diffuses into the matrix and allows the formation of Al_4C_3. No other carbides are detected from the X-ray analysis. Formation of $Al_{3.21}Si_{0.47}$ is also noted. The oxidation reaction which takes place in the melt pool promotes the oxidation of aluminium and silicon in the form of Al_2O_3 and SiO_2, respectively, although these are not detected during the X-ray analysis. As illustrated in the above example, laser alloying and laser cladding can lead to formation of multiple phases completely governed by the process conditions.

7.3.2 Mechanical Properties

With regard to the mechanical properties, hardness is the most widely reported parameter. As the modified layer generally has a gradient of composition, especially in laser-alloyed layer, a gradient in hardness is inevitably obtained. The gradient in the alloyed layer is also responsible for scanty reported literature on fracture toughness (indentation toughness) of the modified layer. Laser transformation hardened steels also exhibit a graded hardness in the heat affected zone (HAZ) underneath the hardened layer. However, such gradient is normally not noticed in laser-cladded layer. Hardness of a wide variety of laser-modified layers has been reported in literature. Although different systems investigated and the varying process conditions preclude a comparison, a compilation of hardness obtained for various modified layers is made in Table 7.2 [38, 39, 41–55]. Depending on the resulting microstructure and phase constitution, the hardness of the modified

Table 7.2 Compilation of hardness of various laser modified layers

Name of the investigators	Laser processing system	Hardness (HV)
Jiang et al. [39]	Nitriding of Ti–6Al–4V	1,100 ± 25
Man et al. [41]	Ti and Sic alloying of Al6061 alloy	540 ± 20
Kwok et al. [42]	NiCrSiB alloying of UNSS31603	380 ± 20
Tassin et al. [43]	Laser surface processing of 316L SS with mixtures of Ti and Sic and Cr_2C_3 and Cr	450 ± 20
Fu and Batchelor [44]	Laser alloying with Ni and Cr of AA6061	320 ± 20
Wang et al. [38]	Laser melted spray coating of amorphous Fe based alloy	850 ± 50
Khedkar et al. [45]	Chromium laser alloyed Cr–Mo steel	591
Shamanian et al. [46]	Austenite steel cladding on ductile cast iron	1,200
Grenier et al. [47]	Ti laser gas carburised	1,800 (KHN)
Guo et al. [48]	Ti laser alloyed with Al	600 ± 50
Staia et al. [49]	Cast Al alloy laser alloyed with WC–Al–Mg powder	600
Datta Majumder and Manna [50]	Pure Cu laser alloyed with Cr	220
Datta Majumder and Manna [51]	304 SS laser alloyed with Mo	700
Datta Majumder and Manna [52]	Ti laser alloyed with Si and Al	700–750
Manna et al. [53]	Plain carbon steel laser cladded with Fe–BC–Si–Al–C	1,150
Persson et al. [54]	316l SS laser cladded with Stellite	700

surfaces can widely vary but the above table gives an idea of the large volume of data that exists. However, there is genuine shortage of data related to toughness of the modified layers. The variation of microhardness as function of depth beneath the laser-melted surface is shown in Fig. 7.13 [39]. Figure 7.13a shows the influence of laser power on the hardness profiles, whereas Fig. 7.13b details the role of scan speed on hardness. Clearly the depth of molten pool increases with increase of laser power and decrease of scan speed.

7.4 Tribology of Laser-Modified Surfaces

Study of tribology of laser-treated surfaces concerns with sliding wear, abrasive wear and erosive wear. Reported investigation on fretting wear is very limited and hence it is not discussed in this section. Most of the study with abrasive wear is on three body abrasion. The applied load and the abrasive give rise to high stress abrasion and low stress abrasion. Solid particle erosion and cavitation erosion are the main subject matters of erosive wear. Other forms of erosion such as rain drop erosion, liquid metal erosion, etc. of laser treated surfaces are not touched upon.

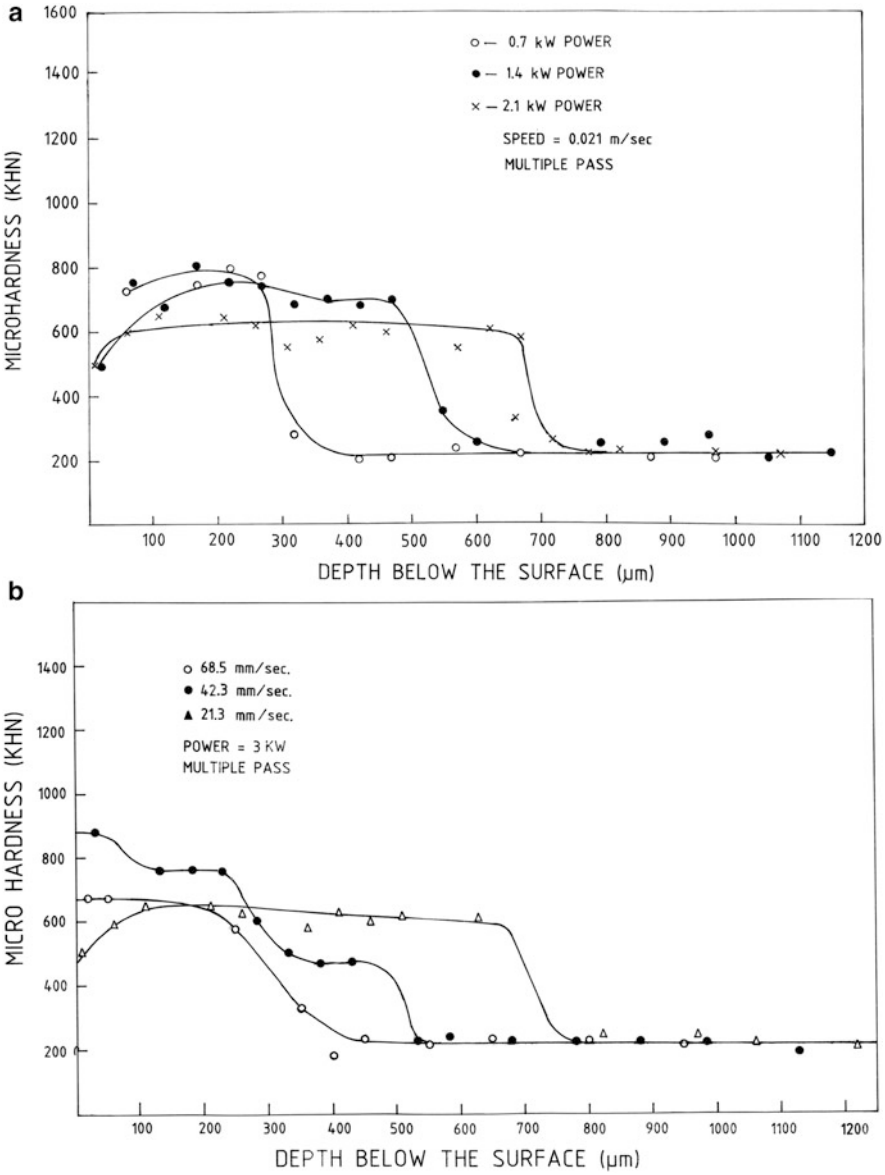

Fig. 7.13 Variation of microhardness as function of depth beneath the laser-melted surface [39]

7.4.1 Sliding Wear

Although tribology of laser-modified surfaces has been studied quite comprehensively, sliding wear of laser-treated surfaces has received the maximum attention.

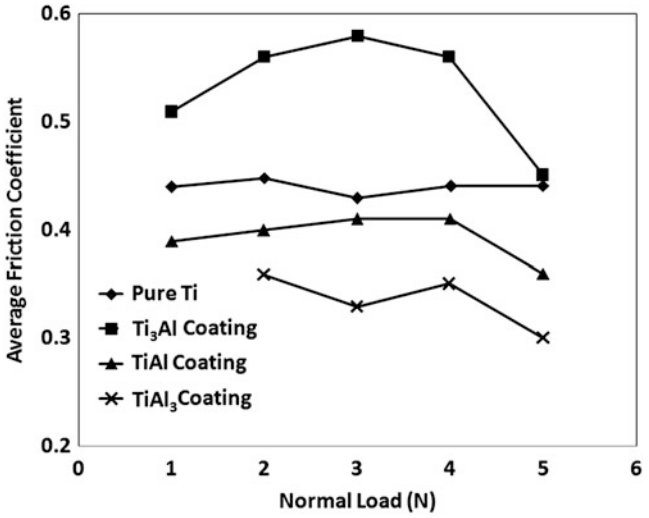

Fig. 7.14 Variation of friction coefficient as function of normal load for various titanium aluminide coatings [48]

The sliding wear characterization is also confined primarily to unidirectional sliding wear and much less study corresponds to reciprocating wear.

7.4.1.1 Friction Response

The impressive amount of data available on the friction response of laser surface-modified layers permits an attempt to generalise the influence of various wear and/or laser processing conditions on friction behaviour of laser-modified surfaces. The influence of applied load on the friction coefficient can be found in the work of Geo et al. [48]. Titanium aluminide coatings were in situ synthesised on a pure Ti substrate by laser alloying a preplaced Al powder and the average friction coefficient of the resulting layer as a function of load is presented in Fig. 7.14. Although $TiAl_3$ exhibited the lowest friction coefficient, the friction coefficient did not follow any specific trend. Rather, it can be concluded that friction coefficient is not governed by applied load. This behaviour can be explained by the fact that the friction coefficient (μ) in case of rough contacting surfaces is given by

$$\mu = \mu_{ad} + \mu_{grov} \tag{7.18}$$

where μ_{ad} is the friction coefficient due to adhesion and μ_{grov} is friction coefficient due to grooving. The adhesion component can be expressed by the following relation [56]:

$$\mu_{ad} = \frac{\tau_m}{H} \tag{7.19}$$

where H is the hardness of the softer material and τ_m the shear strength of the contacting asperities and the shear strength is known to depend on the work of adhesion of the mating materials [57]. Further, the friction coefficient due to grooving is given by

$$\mu_{grov} = \frac{\tau_c \times A}{L} \tag{7.20}$$

where L is the applied load, A is the area sheared plastically by an abrasive particle and τ_c is the critical shear strength of the modified layer. From the above equations, it is clear that at low applied load, the grooving component dominates while when load is increased the adhesion component dominates. Thus, the friction coefficient remains more or less unaltered. Similarly, Dutta Majumder et al. [53] have also noted the load independent friction coefficient of Ti laser surface alloyed (LSA) with Si, Al and Al + Si. In this study, the tribological characteristics of the laser-alloyed samples were investigated to ascertain the variation in wear depth as a function of load and time using a computer-controlled reciprocating ball-on-disc wear testing machine fitted with an oscillating hardened steel ball. A detailed post-wear microstructural analysis was also conducted to determine the mechanism of wear and the role of alloying elements in improving the resistance to wear. The authors have reported that LSA with Si is more effective in improving the wear resistance of Ti than that by Si + Al or Al alone. The enhanced performance in Si surface-alloyed samples has been attributed to the presence of uniformly distributed Ti_5Si_3 in the alloyed zone. Work due to Tassin et al. [43] shown in Fig. 7.15 indicates increase of friction coefficient with increase of hardness. This behaviour is in contrast to Eq. (7.19) which suggests that the friction coefficient should decrease with increase of hardness signifying that the adhesion component plays a nominal role.

Similarly, the influence of sliding speed on friction coefficient is shown in Fig. 7.16. The friction coefficients of laser-processed titanium aluminide coatings were found to decrease drastically with increasing sliding speed. Under identical dry sliding wear conditions, the wear resistance of the titanium aluminide coatings was in the following order: Ti_3Al coating > TiAl coating > $TiAl_3$ coating. The decrease of the friction coefficient with increase of sliding velocity follows the trend described by the equation given below [58].

$$\mu = K_1 - K_2 \mathrm{Ln}(v) \tag{7.21}$$

where μ is the coefficient of friction and v is the sliding velocity. K_1 and K_2 are material-specific constants.

Roughness of the modified surface also plays a crucial role in determining the friction coefficient. Higher roughness typically corresponds to more asperities slope

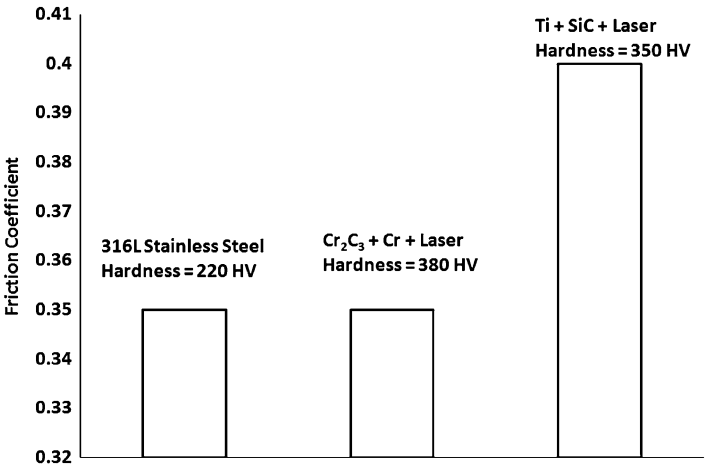

Fig. 7.15 Friction coefficient of various laser surface-alloyed stainless steel showing increase of friction coefficient with increase of hardness [43]

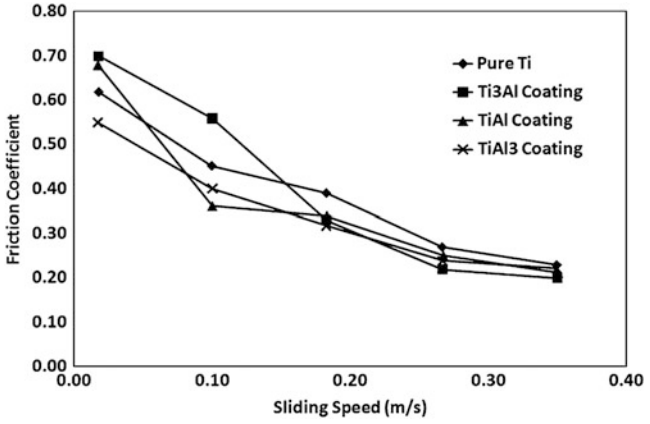

Fig. 7.16 Influence of sliding speed on the friction coefficient of titanium aluminide coatings [48]

angle, which, in turn, increases the friction coefficient. There are two well-established mechanisms responsible for higher friction coefficient being noted in films having higher roughness. The first one is the ratcheting mechanism, where relative motion between two surfaces is achieved by asperities riding over each other. The second is the energy loss mechanism where asperities push each other. In the initial stage of sliding, there can be other operative mechanisms resulting in different trend. Work due to Staia et al. [49] indicated a decrease in friction coefficient with increase in roughness. Their work is presented in Fig. 7.17. This observation, however, is in direct contrast with that reported by many others [53]. The contradicting results of Staia et al. [49] are related to debonding of reinforcing

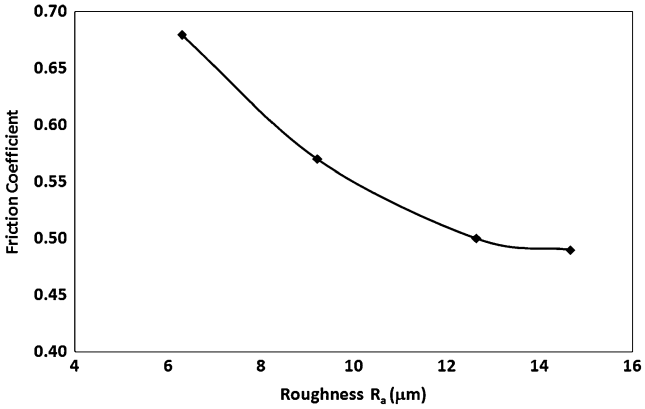

Fig. 7.17 Influence of surface roughness on friction coefficient [49]

WC particles which subsequently act as abrasive particles and thereby increasing friction coefficient.

7.4.1.2 Wear Rate

The wear rates of laser-processed surfaces are determined by wearing conditions. As is the case with other modified surfaces, the wear rate of laser-modified surface increases with applied load as long as the wear is plasticity dominated as per Eq. (7.22) given below:

$$W = k\frac{F}{H} \tag{7.22}$$

where k is the wear coefficient, F is the applied load and H is the hardness of the wearing material. The friction and wear properties of the titanium aluminide coatings at different normal loads and sliding speeds were investigated. It was found that the hardness of the titanium aluminides coatings was in the following order: Ti_3Al coating > TiAl coating > $TiAl_3$ coating. Friction and wear tests revealed that, at a given sliding speed of 0.10 m/s, the wear volume of pure Ti and all titanium aluminide coatings increased with increasing normal load as shown in Fig. 7.18. Such behaviour is consistent with Eq. (7.22) given above.

The laser processing conditions employed are known to influence the wear performance of the modified surfaces. At a given normal load of 2 N, the wear volume of Ti_3Al coating and TiAl coating first increased and then decreased, while the wear volume of $TiAl_3$ coating first decreased and then increased with increasing sliding speed as shown in Fig. 7.19. This behaviour may be related to change of wear mechanism from mild oxidational wear to severe oxidational wear. Another illustration of how the speed at which the modified surface is scanned alters the

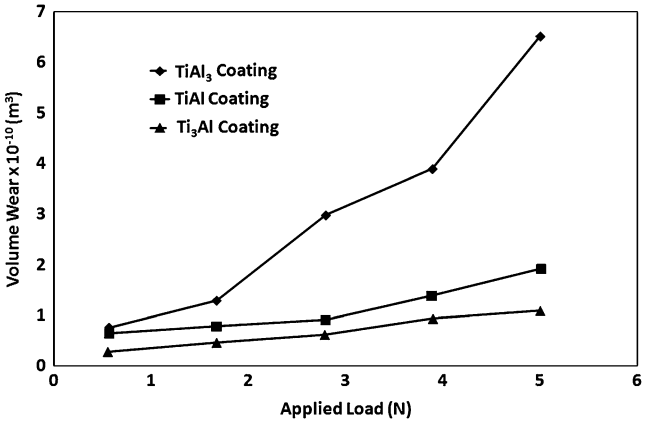

Fig. 7.18 Influence of applied load on the wear rate of laser-treated titanium aluminide coatings [48]

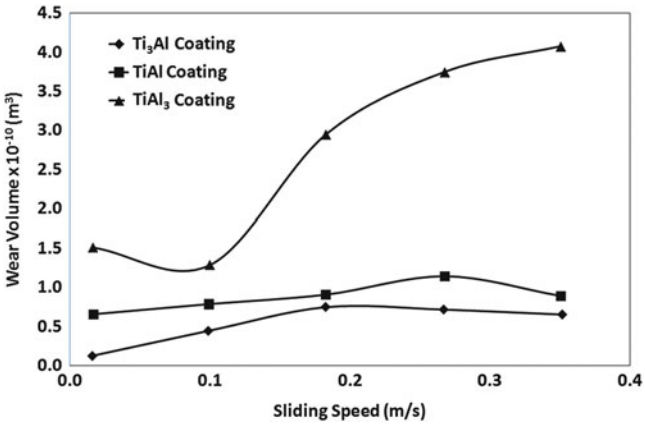

Fig. 7.19 Influence of sliding speed on the wear rate of laser-treated titanium aluminide coatings [48]

wear response of modified surfaces is presented in Fig. 7.20. The wear rate decreases with increase of scan speed. As the scan speed increases, the solidification rate increases thereby resulting in finer microstructure which is often accompanied by superior mechanical properties of modified surface. The improved mechanical properties, particularly increase in hardness, result in reduction of wear rate as per Eq. (7.22) described above.

Radek and Bartkowiak [59] have evaluated the tribological properties of laser-treated and electro-spark-deposited coatings. The tests were conducted for Mo and Cu coatings (the anode) which were electro-spark deposited over a C45 steel substrate (the cathode) and melted with a Nd:YAG laser beam. The coatings after

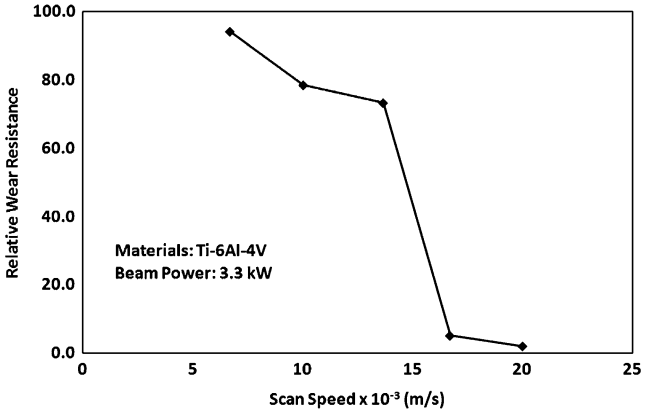

Fig. 7.20 Influence of scan speed at beam power of 3.3 kW on the wear resistance of Ti–6Al–4V alloy [55]

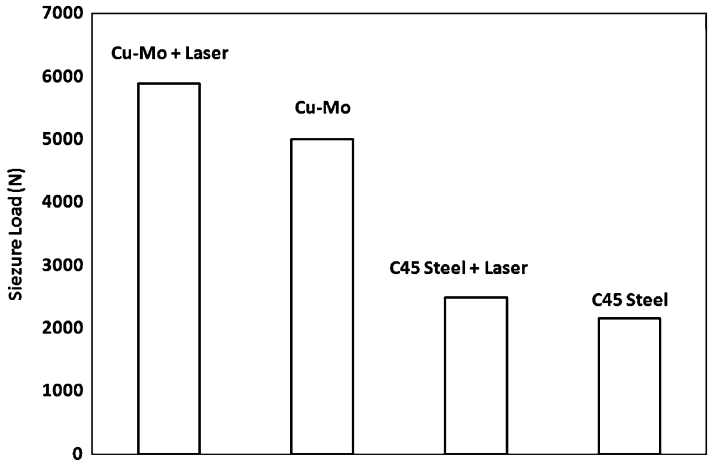

Fig. 7.21 Improvement of seizure load of C 45 steel by laser treatment of Cu–Mo coating deposited by electro spark technique [59]

laser processing are still distinguished by very good seizure load as shown in Fig. 7.21.

Persson et al. [54] examined the frictional behaviour and galling resistance of the laser-processed Fe-based alloy Norem 02 at temperatures ranging from room temperature (RT) to 527 K. Friction and galling testing was performed by sliding two crossed test rods in a load-scanning test rig. The results were compared with those from laser-processed Stellite 21, one of the best low frictions, galling resistant, Co-based alloys known. At room temperature, Norem 02 exhibited excellent sliding performance, comparable to that of Stellite 21, showing a low and stable friction coefficient of 0.25 and revealed no tendency to gall. However, at

temperatures of 427 K or above, the friction coefficient rose to 0.5–0.7 and massive galling was observed. Stellite 21, however, maintained its excellent friction performance even at higher temperatures.

At an intermediate sliding speed and applied load, mild oxidational wear has been reported to become prevalent. The wear rate (W) for mild oxidation is given as [58]

$$W = \frac{FC^2A_o}{vZ_cH_o}\exp\left(-\frac{Q}{RT_f}\right) \tag{7.23}$$

where A_o is Arrhenius constant, Q is the activation energy for oxidation, Z_c is the critical thickness of spalling, T_f is the temperature at the point of contact of the asperities, v is the sliding velocity, C is a constant which depends on the composition of the oxide scale and R is the molar gas constant.

The contact temperature at the asperities, known as flash heating temperature, is given by [58]

$$T_f = T_b + \frac{\mu vr}{2K_e}\left(\frac{H_oF}{NA_n}\right)^{\frac{1}{2}} \tag{7.24}$$

where H_o is the hardness of the oxide scale, N is the total no of the asperities, r is the radius of the contacting area and K_e is the equivalent thermal conductivity.

The oxidation under sliding wear takes place at a rate higher than that observed under static conditions [60–62]. The observed difference is due to change of Arrhenius constant A_o, which depends on material and wearing condition [63]. However, the activation energy for oxidation Q remains unchanged [64]. Hence, further discussion on lowering the wear rate will be confined to the activation energy Q and the critical thickness of spalling (Z_c). Examination of the activation energies for oxidation (Q) for a large number of oxide scales [58, 64] indicates that the activation energies for oxidation are high for Al_2O_3 and Cr_2O_3 scale formation. Hence, many surface engineering solutions to improve wear resistance in this regime involve forming of Al-or Cr-rich layers. This can be achieved by laser surface alloying.

Hirose et al. [65] have reported improved wear performance on alloying Ti with Al using a laser. When Ti undergoes mild oxidational wear, it results in the formation of TiO_2 and wears through a spallation mechanism. When alloyed with Al by laser surface alloying, a protective Al_2O_3 scale forms. Since the activation energy for formation of Al_2O_3 is much higher compared to TiO_2, the growth of this oxide scale is much slower. Thus, it takes a long time for the critical spalling thickness to be attained leading to reduced wear rate. Similarly, Tau and Doong [66] found that the chromium-alloyed surface exhibited higher wear resistance compared to untreated steel for a given hardness and structure. This behaviour can also be attributed to the fact that the chromium-rich layer formed a Cr_2O_3 scale, which exhibited better adhesion to the substrate than the Fe_2O_3 scale formed on the

untreated steel. Isawane and Ma [67] also reported an improved wear performance of stainless steel when coated with Cr and Ni.

The third method of reducing the wear rate is to increase the critical thickness of spalling. For a given oxide scale substrate system, the critical thickness for spalling (Z_c) can be increased by the following means:

1. Adding *Y*, Hf or rare earth elements on the surface [68, 69].
2. Ensuring fine dispersoids near the surface, either by internal oxidation or by using mechanically alloyed material [70].
3. Aluminising with noble alloying elements, e.g. Pt, Au, Ag, etc. as such addition results in cleaner oxide formation [71–73].

Addition of *Y*, Hf and rare earth elements is known to increase the adhesion of the oxide scale, and this has been attributed to the following:

1. Scale grows into the substrate at scale–metal interface resulting in mechanical pegging [74].
2. Voids generation at the scale–metal interface is prevented by vacancy accommodation [75].
3. Grains become finer and grain boundary diffusion coefficient increases, thereby promoting stress relief by cobble creep [76].
4. Acting as nucleation sites and producing a fine grained scale, the dispersoids block the boundaries and sulphur segregation at the scale–metal interface is prevented. This prevents embrittlement at the scale–metal interface. This acts as oxygen active dopants [77].

The increase in critical thickness of spalling, resulting in increase of wear resistance, is reflected in the work of Wang et al. [38] who noted an increase in wear resistance with laser surface alloying of substrate, a low carbon steel by CeO_2. Their results illustrated in Fig. 7.22 depict wear rate as function of hardness. Clearly a lower wear rate can be seen with a CeO_2-alloyed surface. They attributed this observation to refinement of microstructure, strengthening and purification of the grain boundary and improvement in the morphology and distribution of eutectics. These refinements result in a more adherent oxide scale which, in turn, improves the wear resistance.

In order to improve the sliding wear resistance of stainless steel components, carbide-hardened surfaces were produced on AISI 316L austenitic stainless steel employing laser surface alloying by Tassin et al. [43]. Different powdered precursors (CrC, a mixture of CrC and Cr and a mixture of Ti and SiC) were applied to the steel surface and irradiated using a continuous wave 300 W Nd–YAG laser. The surface alloys resulting from the incorporation of CrC, alone or mixed with chromium, were composed of austenite (γ) dendrites surrounded by a γ-M_7C_3 eutectic (M = Fe or Cr) and their microhardness ranged from 380 to 450 HV. Superficial hardening by titanium carbide was obtained using a mixture of Ti and SiC powders as precursors. Ti and SiC particles dissolved in the melted pool, leading to the precipitation of fine TiC particles during solidification. The microhardness of the surface alloy was about 350 HV. For both chromium carbide

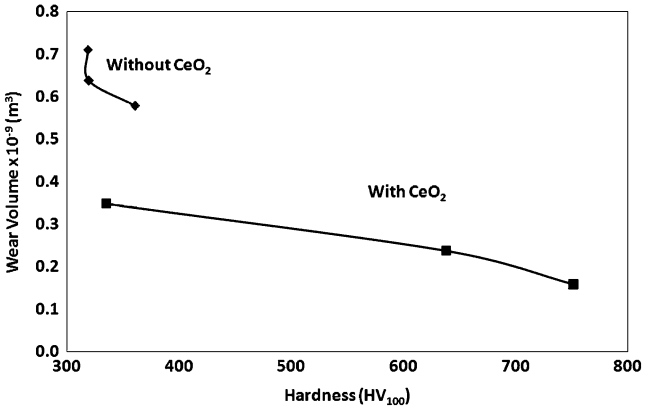

Fig. 7.22 Improvement of wear resistance of low carbon steel 1020 by addition of CeO_2 employing laser [38]

and titanium carbide surface-alloying treatments, a noticeable improvement in the sliding wear resistance of AISI 316L stainless steel was noted.

A significant amount of work has been reported on improvement of tribological properties on introduction of carbon on the ferrous materials by laser surface alloying, either using graphite or melting in presence of CO_2 or acetylene [78–80]. Laser-borided single-phase iron has been shown to be superior in terms of sliding wear resistance and rolling contact fatigue resistance to traditionally single-phase-borided samples. Laser alloying of high speed steel by BN and Ti/BN resulted in increased tool life [81]. Laser surface alloying of Cu–Ni alloy with boron powder using a defocused CO_2 laser has been reported to increase wear resistance as high as 40 times [82]. Gulan et al. [83] found improvement in wear by scratching of laser-alloyed Al80 as shown in Fig. 7.23. According to their result, laser alloying with Al results in marginal improvement of wear resistance. Alloying with Ni and Si led to limited enhancement, in spite of improved hardness. This fact is attributed to formation of brittle phases such as $Mg_{17}Al_{12}$, Mg_2Ni, Mg_2Si, etc. However, alloying with Cu was found to yield significant improvement in wear resistance.

The potential of producing rapidly solidified microstructures with enhanced hardness and wear resistance by laser cladding of Co, Fe and Ni base alloys on traditional substrate materials has also been demonstrated by several researchers [13, 84–86]. Belmondo and Castagna have successfully laser cladded a mixture of Cr–Ni–Mo and Cr–carbide on mild steel with increased wear performance [87]. A study by Singh and Majumder [88] has shown that laser cladding of Fe–Cr–Mn–C on steel yields a fine duplex microstructure of fine grain ferrite matrix with M_6C and M_7C_3 carbide precipitates which leads to superior wear properties compared to Stellite 6. Use of Cr_3C_2 and Mo_2C clad materials is found to yield a β-Ti + TiC microstructure which is desirable to improve wear characteristics [89].

A comparison between the wear rates of laser surface-hardened and laser surface-melted surfaces has been made by Roy and Manna [90]. In their study, an

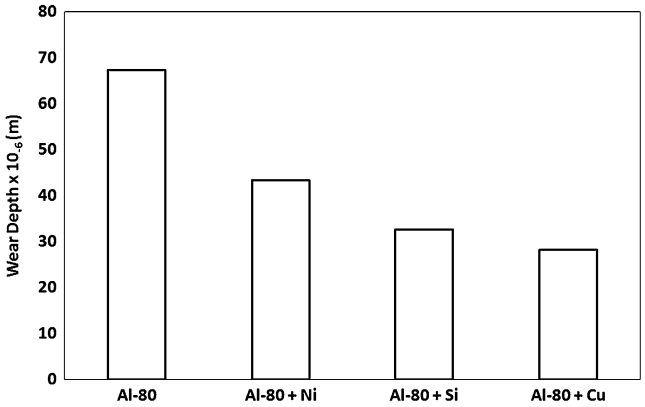

Fig. 7.23 Bar diagram showing improvement of wear resistance by laser surface alloying of aluminium alloy Al 80 [83]

attempt has been made to evaluate the scope of enhancing wear resistance of austempered ductile iron by laser surface melting (LSM) and laser surface hardening (LSH). A detailed study concerning microstructural evolution and mechanical properties following LSM and LSH indicates that LSM develops a relatively low microhardness in the near-surface region and a predominantly austenitic microstructure in the laser-melted zone. On the other hand, LSH, compared to LSM, results in a higher hardness and a more uniform microhardness profile due to a primarily fine martensitic microstructure in the laser-hardened zone. Careful X-ray diffraction analyses coupled with microstructural studies reveal that diffusion of carbon from graphite is responsible for a higher volume fraction of retained austenite and lower hardness in the laser-irradiated zone following LSM as compared to LSH. Furthermore, LSH leads to development of residual compressive stress, while LSM produces residual tensile stress on the surface. Finally, adhesive wear tests with a pin-on-disc machine and subsequent microstructural analyses show that LSH is more appropriate than LSM to enhance adhesive wear resistance of austempered ductile iron. Figure 7.24 presents a SEM image of a worn surface of a laser surface-melted sample showing delamination or removal of material during adhesive wear at a load of 5 kg. The high magnification scanning electron micrograph (Fig 7.24b) of the wear debris substantiates that loss of metal occurs primarily by the propagation of micro-cracks at the surface. The latter may be fatigue-cracks initiated at the sub-surface or may initiate from the austenite–martensite interface where deformation constraints are maximum. Improved wear performance of laser surface-hardened 52100 steel has also been demonstrated by Basu et al. [91]. Similarly, Padmavati et al. [92] found that laser surface melting of magnesium alloy improved wear resistance. Other studies have shown that laser surface alloying and laser composite processing [93, 94] result in improved wear resistance of aluminium alloys.

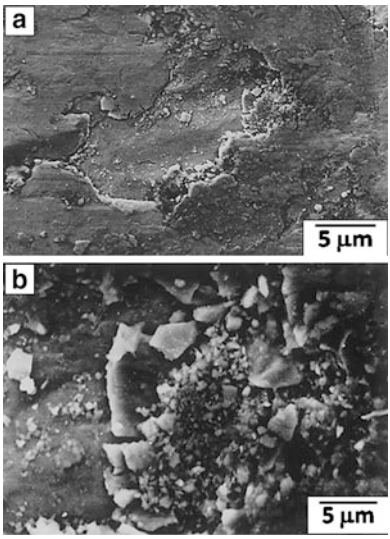

Fig. 7.24 SEM image of a worn surface of a laser surface-melted austempered ductile cast iron [90]

7.4.2 Abrasive Wear

Laser surface modification offers a promising route for improving the abrasive wear resistance of materials. Abrasive wear resistances of a variety of steels and other materials have been improved by laser surface modification. The abrasive wear rate of laser transformation hardened steels of varying carbon content, along with their corresponding hardness, is illustrated in Fig. 7.25. Clearly, the abrasive wear resistance increases with increase in hardness of the laser surface-modified steel layer in accordance with Eq. (1.16) of Chap. 1.

Jiang et al. [55] nitrided Ti–6Al–4V alloys using a laser in a gaseous nitrogen environment. A significant improvement in abrasive wear resistance upon laser nitriding was noted. The abrasive wear rate is also as expected governed by the processing parameters, for example, as shown in Fig. 7.26, the abrasive wear resistance decreases with increasing scan rate. This is attributed to the unique microstructure of the 'in situ' laser surface-alloyed composite coatings. The as-solidified dendritic TiN reinforcements strongly embedded in the matrix provide the laser surface-alloyed coatings excellent resistance. The volume fraction of the 'in situ'-solidified TiN reinforcement and thereby the wear resistance of the laser surface-alloyed composite coatings can be easily controlled by varying the laser surface alloying parameters.

The gas composition during laser surface gas alloying is also known to govern the abrasive wear behaviour. According to Grenier et al. [47], laser gas alloying of Ti result in increase in abrasive wear resistance as shown in Fig. 7.27. The best wear resistance was found when the surface was alloyed with a mixture of carbon monoxide and nitrogen gas. The best abrasive wear resistance was exhibited by the layer having highest hardness and it is plausible that the mixed carbides and

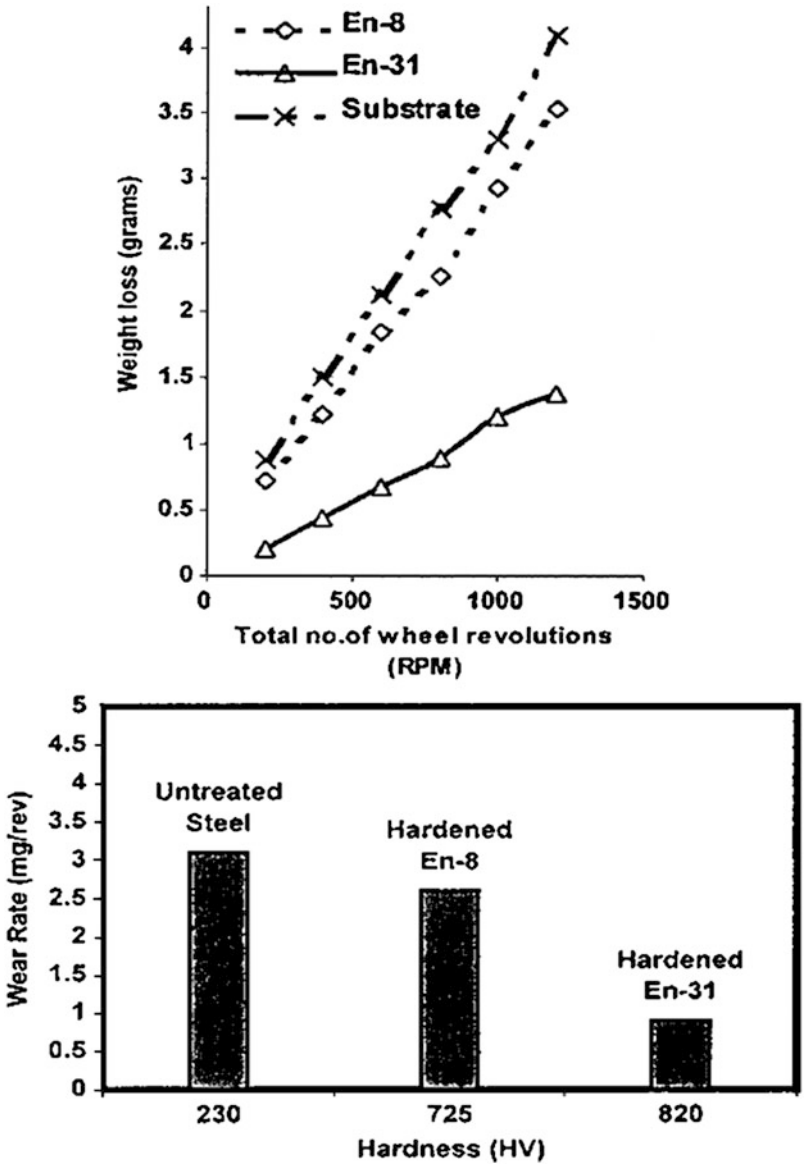

Fig. 7.25 Abrasive wear rate of laser transformation hardened steels of varying carbon content along with their corresponding hardness

nitrides that result in alloyed layer when the above gas mixture is used are responsible for the enhanced properties.

Hybrid processing by combining laser treatment with another coating process has great technological potential. For example, laser glazing of plasma-sprayed and

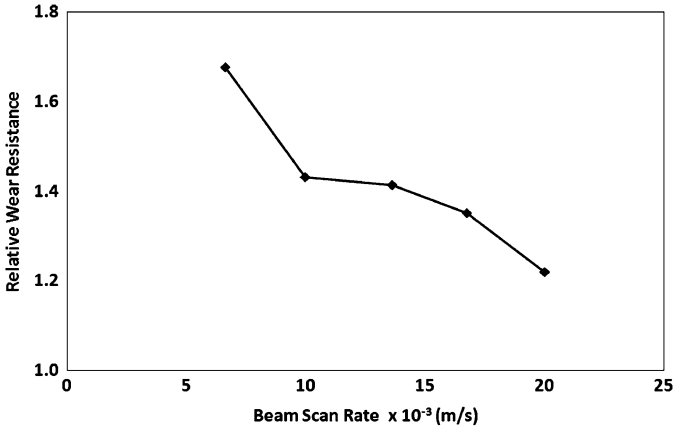

Fig. 7.26 Influence of beam scan speed on relative abrasive wear resistance of Ti–6Al–4V [55]

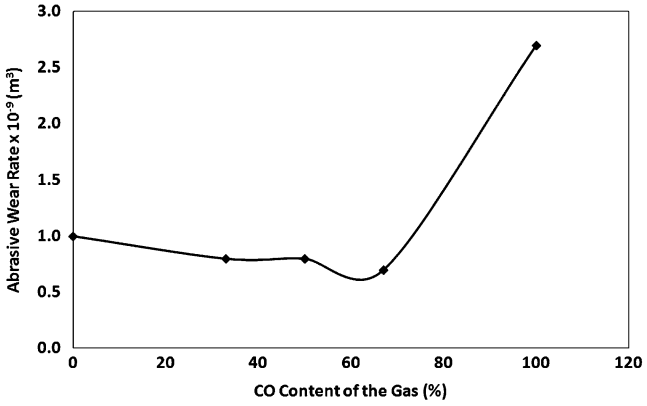

Fig. 7.27 Influence of gas composition (CO content) on the abrasive wear rate of laser gas-alloyed Ti [47]

detonation-sprayed coatings exhibited improved abrasive wear resistance as compared to as sprayed coating. Such behaviour is shown in Fig. 7.28. Further, laser-glazed detonation-sprayed coatings also exhibited better wear resistance than as-sprayed coating. However, the property enhancement was not as pronounced as in the case of laser post-treatment of plasma-sprayed coatings as the detonation-sprayed coatings are characterised by negligible porosity and provide little opportunity for further improvement. The result also highlights the importance of glazing power and speed in relation to final performance of the treated layer.

Rieker et al. [95] found enhancement in abrasive wear resistance of ferritic stainless steel by laser alloying with Mo as well as Mo + B. Laser-treated boronised surface exhibits improved abrasive wear rate at low laser power and higher wear rate at high laser power. This behaviour is illustrated in Fig. 7.29. Boas and

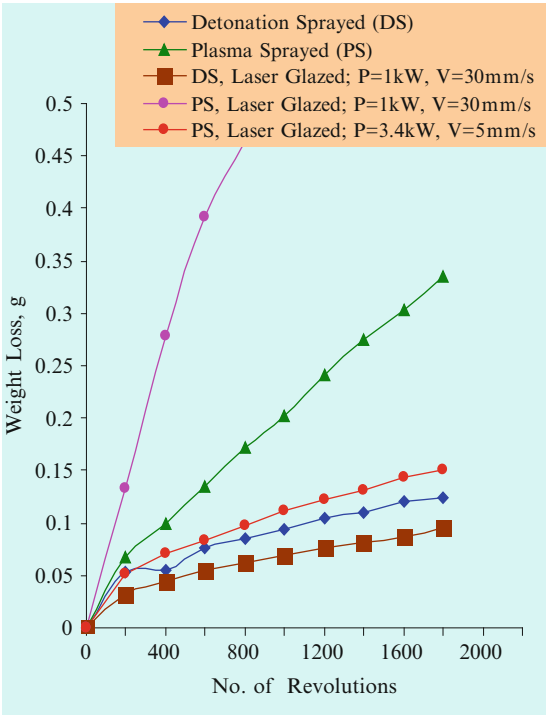

Fig. 7.28 Abrasive wear resistance of laser-glazed plasma-sprayed and detonation-sprayed coatings

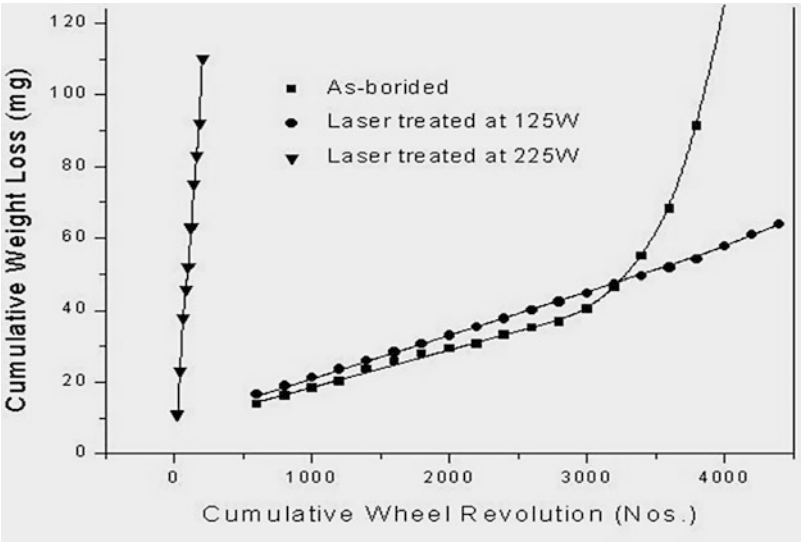

Fig. 7.29 Abrasive wear resistance of laser-treated boronised steel

Bamberger [96] also reported improved abrasive wear performance of low alloy steel by hybrid processing which consists of plasma spraying of triballoy T-400 followed by laser surface melting.

7.4.3 Erosive Wear

Significant work has been done on the erosion, including cavitation erosion of laser surface-modified materials. Laser surface modification of NiCrSiB coating (Ni-16.5Cr-15.5Fe-3.5Si-3.8B-0.1C) on austenitic stainless steel UNS S31603 (Fe-17.6Cr-11.2Ni-2.5Mo-1.4Mn-1.4Cu-0.4Si-0.03C) was achieved by using a 2-kW continuous wave Nd–YAG laser by Kwok et al. [42]. The cavitation erosion of the laser surface-modified UNS S31603 was studied by means of a 20-kHz ultrasonic vibrator at a peak-to-peak amplitude of 30 mm. The NiCrSiB alloy layer was flame sprayed on the surface of UNS S31603 stainless steel. The surface was then scanned with the laser beam. The melt depth and dilution of the sprayed layer with the substrate material increased with decrease in scan speed. At low dilution ratio of sprayed layer thickness to melt depth, less secondary phases such as CrB, CrB_2, Fe_2B and $M_7(CB)_3$ and lower hardness were observed in the laser-modified layer. The cavitation erosion resistance (reciprocal of the mean depth of penetration) of the laser-modified specimen with a dilution ratio of 0.65 was improved by 2.7 times as compared with that of the as-received UNS S31603 specimen. The cavitation erosion resistance of the laser surface-modified specimen with dilution ratio of 0.88 was improved fourfold as compared with that of the as-received UNS S31603 and very close to that of super duplex stainless steel UNS S32760 (Fe-25.6Cr-7.2Ni-4Mo-0.6Mn-0.7Cu-0.8W-0.3Si-0.2N-0.03C). Finally, it is noted that the cavitation erosion resistance is directly related to the hardness of the surface-alloyed stainless steel as illustrated in Fig. 7.30.

The materials loss in case of metallic materials during erosion at ambient conditions is primarily by formation of lip and their subsequent fracture. As per the localization model, it is demonstrated by Sundararajan and Roy [97] that the erosion rate is given as

$$E \propto \left(\frac{L}{r}\right)^3 \left(\frac{\Delta\varepsilon_m}{\varepsilon_c}\right) \tag{7.25}$$

where L is the depth to which plastic deformation extends beneath the surface, r is the radius of the impacting particles, $\Delta\varepsilon_m$ is the mean strain increment for each impact and ε_c is the critical strain for onset of localization. If the constitutive equation of plastic flow is given as

$$\sigma = K\varepsilon^n(1 + CT) \tag{7.26}$$

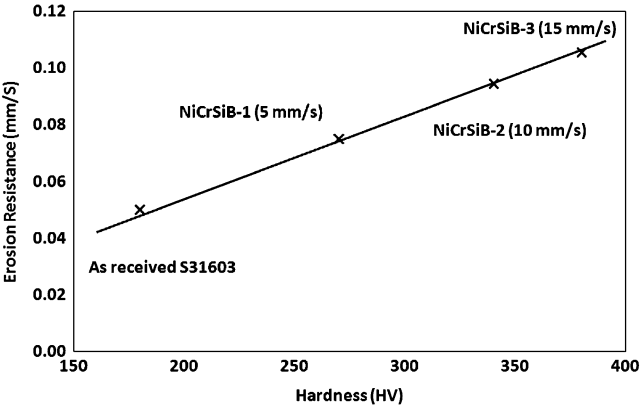

Fig. 7.30 Influence of hardness on cavitation erosion resistance of NiCrSiB coating [42]

where K is the strength coefficient, C is the temperature coefficient of flow stress and n is the strain hardening exponent, ε_c can be obtained as

$$\varepsilon_c = \left[\frac{n\rho C_P}{KC}\right]^{\frac{1}{n+1}} \tag{7.27}$$

where ρ is the density of the eroding material and C_P is the specific heat. K can be replaced by the melting point (T_m) of the eroding materials according to

$$C = \frac{4.5}{T_m} \tag{7.28}$$

Thus, the critical strain for localization can be written as

$$\varepsilon_c = \left[\frac{n\rho C_P T_m}{4.5K}\right]^{\frac{1}{n+1}} \tag{7.29}$$

Or

$$\varepsilon_c \cong \frac{n\rho C_P T_m}{4.5K} \tag{7.30}$$

since erosion takes place at high strain and n at high strain is normally very low thereby making $n + 1$ nearly equal to 1. From Eq. (7.25), it is clear that, for a given eroding condition, L, ρ and $\Delta\varepsilon$ are constant. Thus the erosion rate is inversely proportional to the critical strain for localization and this critical strain for flow localization is directly proportional to melting temperature. In other words, the

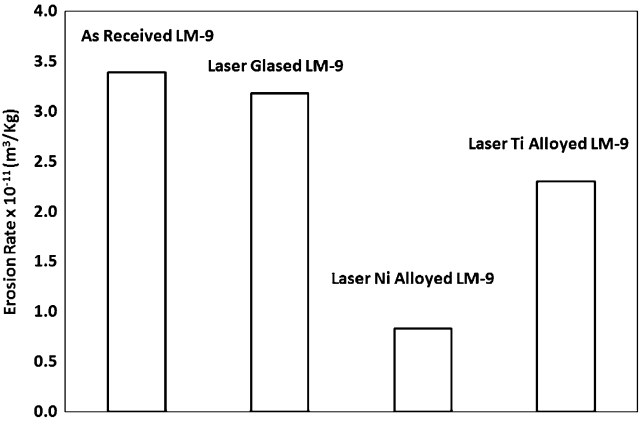

Fig. 7.31 Improvement of erosion resistance of laser-alloyed LM-9 with Ti and Ni [98]

erosion rate is inversely proportional to the melting temperature of the eroding materials as given below

$$E \propto \frac{4.5K}{n\rho C_P T_{\mathrm{m}}} \tag{7.31}$$

Hence, higher the melting temperature of the surface, lower is the erosion rate. Roy et al. [98] employed this concept to laser surface alloying of Al alloy LM-9 by Ni and Ti and found improved erosion rate. Their result is presented in Fig. 7.31. Erosion resistance of laser-glazed, laser Ni-alloyed and laser Ti-alloyed LM-9 improved by 6.2 %, 76 % and 32 % respectively.

The study by Datta Majumder and Manna [51] concerns laser surface alloying (LSA) of AISI 304 stainless steel (304-SS) with pre-deposited Mo (by plasma spraying) to enhance erosion–corrosion resistance of the substrate. The optimum LSA conditions in terms of pre-deposit thickness, laser power density q and scan speed v have been identified to achieve the desired microstructure, composition and mechanical properties. LSA under such optimum conditions significantly improves the erosion–corrosion resistance in 20 wt.% sand in 3.56 wt.% NaCl solution as depicted in Fig. 7.32. Thus, it is concluded that LSA of 304-SS with Mo is an appropriate technique to enhance the resistance to erosion–corrosion in stainless steel. Datta Majumder and Manna [50] also explored the possibility of improving erosion resistance of Cu by laser surface alloying with Cr. As shown in Fig. 7.33, an improvement in room temperature and elevated temperature erosion resistance is noted. The above observation can be explained in terms of erosion behaviour at elevated temperature. As such high temperature, erosion will occur primarily by spallation of oxide scale and therefore the erosion rate will be determined by the steady state oxide scale thickness which is governed by the balance of growth of oxide scale by oxidation and erosion of oxide scale due to impact. If it is assumed

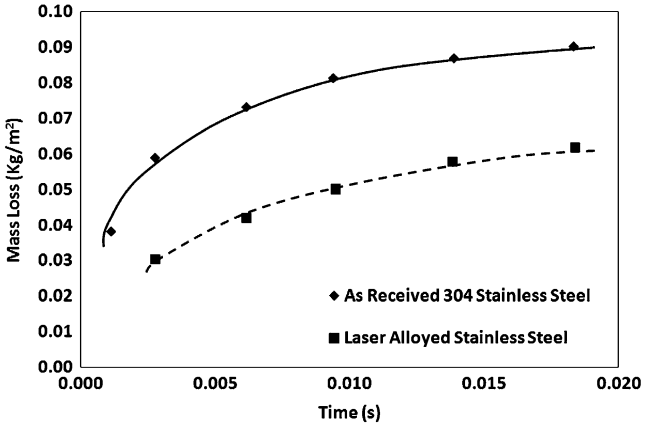

Fig. 7.32 Improvement in erosion–corrosion resistance of laser surface-alloyed 304 stainless steel with Mo in 20 wt.% sand in 3.56 wt.% NaCl solution [51]

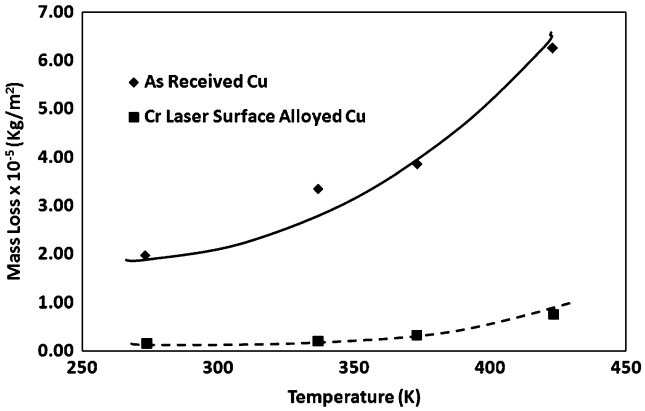

Fig. 7.33 Improvement of room temperature and elevated temperature erosion resistance of copper laser surface alloyed with Cr [50]

that the oxide scale which forms on the eroding material during erosion is adherent and sufficiently ductile to withstand repeated impact without developing cracks, steady-state oxide scale thickness can be defined. It can be assumed that the oxidation of the eroding material follows parabolic kinetics given by the Eq. (7.32)

$$\Delta m^2 = K_{\mathrm{p}}^{\mathrm{o}} t \tag{7.32}$$

where Δm is the mass gain experienced per unit area due to intake of oxygen to form the oxide scale, $K_{\mathrm{p}}^{\mathrm{o}}$ is the parabolic rate constant and t is the time of exposure. The parabolic rate constant is usually expressed in the form

$$K_{\mathrm{p}}^{\mathrm{o}} = A_o \exp\left(\frac{-Q}{RT}\right) \tag{7.33}$$

where A_o is the Arrhenius constant, Q is the activation energy for oxidation, R is the gas constant and T is the absolute temperature.

In order to represent the E–O interaction in mathematical terms, one needs the rate of growth of the oxide scale thickness with time rather than the weight gain given by Eq. (7.32). As noted by Lim and Ashby [57], once the composition of the oxide scale is known, Eq. (7.32) can be transformed to give

$$Z^2 = 2K_{\mathrm{p}}t \tag{7.34}$$

$$K_{\mathrm{p}} = 0.5C^2K_{\mathrm{p}}^{\mathrm{o}} \tag{7.35}$$

where C is a constant for a given oxide composition (with units is m^3/kg). K_{p} is usually referred to as the scaling constant. A value appropriate to erosion conditions should be chosen for K_{p}, since Levy et al. [99] have clearly demonstrated that the oxide scales grow much more rapidly under erosion conditions as compared to static conditions. From Eq. (7.34), the rate of increase of oxide scale thickness with time is given as

$$\frac{\mathrm{d}Z}{\mathrm{d}t} = \frac{K_{\mathrm{p}}}{Z} \tag{7.36}$$

If E_{o} is assumed to be the erosion rate of the oxide scale and F the particle flux rate given by the ratio of particle feed rate (f) to the eroded area, then the rate of decrease of the oxide scale thickness due to its erosion is obtained as

$$\frac{\mathrm{d}Z}{\mathrm{d}t} = -\frac{E_{\mathrm{o}}F}{\rho_{\mathrm{o}}} \tag{7.37}$$

where ρ_{o} is the density of the oxide.

Finally, a situation will arise when the oxide growth by oxidation [Eq. (7.36)] will be equal to the oxide removal by erosion [Eq. (7.37)]. Under such condition, the steady state oxide thickness (Z_{ss}) can be obtained as

$$Z_{\mathrm{ss}} = \frac{K_{\mathrm{p}}\rho_{\mathrm{o}}}{E_{\mathrm{o}}F} \tag{7.38}$$

Hence, the steady state oxide thickness increases with increasing temperature (through K_{p}), decreasing oxide erosion rate and decreasing particle flux rate. It should be mentioned that E_{o} in Eq. (7.38) represents the erosion rate of pure oxide. Now K_{p} can be expressed as

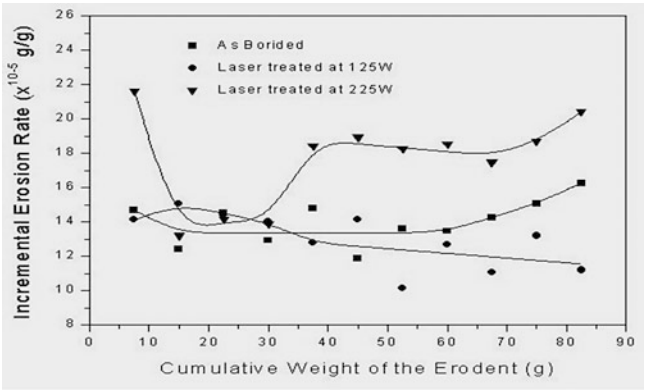

Fig. 7.34 Effect of hybrid processing such as boronising followed by laser treatment on erosion resistance of steel

$$K_{\mathrm{p}} = A_o \mathrm{Exp}\left(-\frac{Q}{RT}\right) \tag{7.39}$$

where A_o is Arrhenius constant and Q is the activation energy for oxidation. From Eq. (7.39) the higher the value of Q, lower is the value of K_{p} and hence lower the Z_{ss} or erosion rate. The substrate Cu will form a CuO scale and Cr-alloyed surface will form a Cr_2O_3 scale. The activation energy for anion diffusion for formation of CuO and Cr_2O_3 scales are 36,100 and 61,100 cal/mol respectively. Hence, the steady state thickness of the oxide scale and, in turn, the erosion rate is significantly higher for Cu-alloyed surface than for a Cr-alloyed surface.

The influence of laser processing conditions on the erosion rate can be seen from Fig. 7.34 in case of a hybrid laser process in which the steel was first boronised and the boronised surface was then modified with a laser. Subsequently the modified surface was subjected to solid particle erosion. The surface modified at a lower laser power was found to exhibit an erosion rate lower than the as-boronised surface. However, when the boronised surface is laser processed at a higher power, the erosion rate is found to be higher than the as-boronised surface.

7.5 Applications of Laser Surface-Modified Components

Laser surface modification is suitable for a wide range of materials and the process can address diverse degradation modes. The earliest industrially accepted applications have involved laser transformation hardening or laser remelting. For example, an image of a laser surface-remelted camshaft is presented in Fig. 7.35. Laser surface melting of a cast iron camshaft has already been commercialised [100]. Similarly there are numerous other applications that have been successfully

Fig. 7.35 An image of cross section of laser surface-remelted camshaft

realised in the author's laboratory such as laser hardening of steam turbine blades, laser remelting of camshafts, etc.

The materials that can successfully be modified using a laser include metals, intermetallics and ceramics. Although the generic applications of laser cladding and laser surface alloying are similar, the fact that there is negligible dilution of clad materials from the substrate makes laser cladding better suited for most tribological applications. However, as laser surface alloying involves addition of relatively lower amounts of the alloying element into the substrate, it can also play crucial role in conserving expensive scarce material. Stellite cladding has been successfully carried out on the surface of valve seat rings and steam generator turbine blades. Silver and copper cladding is also routinely done for electrical contactor industry. For aircraft industries, wear facing using a laser has been performed for tracks of aircraft carrier launch rails and naval aircraft skid plates. The shroud interlocks between turbine blades are laser cladded to reduce wear that may occur when the cold engine is heating up to fill the expansion gap between the blades. Rolls Royce has introduced laser cladding for hardfacing turbine blades of aero engines [100]. Laser cladding is also employed for repairing damaged zones of high temperature turbine blades [101]. In the nuclear industry, laser surface modification is done for nuclear support plates, nuclear displacement rod drive mechanisms, nuclear pump seal rings, etc. Laser cladding of municipal combustor waste components and submarine shaft seals has been successfully developed. Toyota R&D has developed laser cladding of copper base alloys on the valve seat with considerable improvement of adhesive and abrasive wear resistance over a range of temperatures [102]. Laser cladded Stellite 6 on valves of diesel engines for ships made of Nimonic80 is shown in Fig. 7.36.

NiTi is an ideal biomaterial for stents applications. In order to reduce the danger of Ni release, this material can be laser gas nitrided to improve biocompatibility [103]. Hydroxyapatite has also been cladded using a laser onto Ti prosthesis to create a coating which allows tissue growth between the prosthesis and the bone for better fixation [104]. Laser alloying is routinely carried out for making machine readable coinage and other metallic objects [105, 106].

Laser cladding is also increasingly used for reclamation and repair. Laser cladding has been used to rebuild the spline on drive shafts [107]. Similarly,

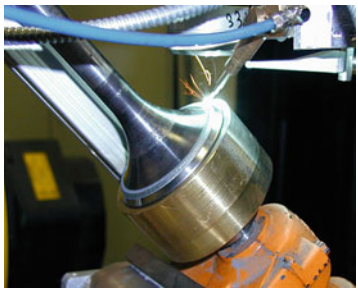

Fig. 7.36 Laser-cladded satellite 6 on valves of diesel engine for ship made of nimonic80

bearings with oil seals used in mining industry are resurfaced by laser cladding. Turbines blades can also be rebuilt at their tips and leading edges. An example of a reclaimed blower shaft of a refinery by laser coating of Stellite is shown in Fig. 7.37 along with a coated and ground portion of the component and the microstructure of the coating.

7.6 Direction of Future Work

The field of hybrid laser processing has attracted growing attention in recent times. As laser is used not only for enhancing wear properties but also for improving corrosion resistance [108, 109], further work on hybrid processing is most relevant. Hybrid processing, such as boronising or thermal spraying followed by laser surface melting has already yielded promising results. Further development and establishment of their applications in the engineering industry are expected in near future as described in several review papers [110, 111]. Other hybrid processes, laser-assisted physical vapour deposition [112, 113], laser-assisted chemical vapour deposition [114, 115], laser-assisted electrodeposition [116, 117], laser-assisted machining [118, 119], laser-assisted drilling [120, 121] and laser-assisted electromachining [122, 123] also provide unique advantages and are worthy of being explored to realise various techno-commercially viable applications.

Advanced processes such as rapid prototyping or low volume manufacturing are another important process that is receiving attention. The rapid prototyping process enables thin-walled, precisely designed metal structures with a density close to 100 % [124] to be obtained. The structures can be produced with the use of a precisely delivered powder introduced through a concentric nozzle into a laser-melted pool (Fig. 7.14). The thickness of the walls produced by rapid prototyping could be as small as the laser spot (from 0.1 mm to a few millimetres). The microstructures of these three-dimensional products are similar to that obtained by powder sintering. The process is applied to form shapes for stamping machines and to fill cracks in damaged bearings, crankshafts and cylinders in automotive engines [125]. Significant development is also taking place in this direction.

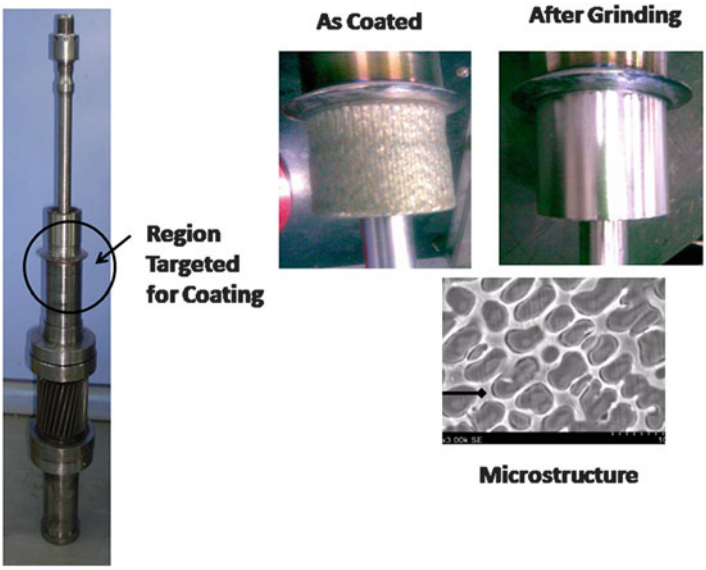

Fig. 7.37 Reclaimed blower shaft of a refinery by laser cladding of Stellite clad and ground portion of the shaft and the microstructure of the clad are also shown

Process automation during laser surface modification is another important area which is getting updated at a rapid pace. The laser beam can be controlled by controlling the power, diameter, structure and location of the beam. Similarly, the traverse speed, vibration, focal point, shroud velocity of the work station can be monitored. The surface absorptivity, seam location, temperature of the work piece can be changed as per requirement. Acoustic signal-based sensors such as mirror, probe, nozzle, workpiece, etc. are currently under investigation. Investigations are also in progress for radiation emission signal-based sensors such as photoelectric, pyroelectric, CCD camera and infrared camera, etc. Other interesting areas are space charge signal-based plasma charge sensor nozzle or ring, Langmuir probe with or without external voltage, etc.

Acknowledgement Various colleagues of one of the authors (SJ) who have been actively involved in R&D as well as application development efforts highlighted in this chapter from Center for Laser Processing of Materials at International Advanced Research Center for Powder Metallurgy and New Materials are sincerely acknowledged.

References

1. Maiman TH (1960) Nature, 6 August
2. Basov NG, Kroklin ON, Popov YM (1961) Sov Phys JETP 13:1320
3. Hall RN, Fenner GE, Kingsley JD, Soltys TJ, Carlson RO (1962) Phys Rev Lett 9:366

4. Nathan MI et al (1962) Appl Phys Lett 1:62
5. Quist TM et al (1962) Appl Phys Lett 1:91
6. Patel CKN (1964) Phys Rev A 136:1187
7. Ewing JJ, Brau CA (1975) Appl Phys Lett 27:330
8. Chande T, Majumder J (1983) Metall Trans B14:181
9. Roy M, Bharti A (2000) In: Proceedings of 3rd workshop on application of laser in mechanical industry, February, Jadavpur, Calcutta
10. Bharti A, Sivakumar R, Goel DB (1989) J Laser Appl 5:43
11. Kovalemko VS, Volgin VI, Mixhailov VV (1977) Tech Organ Proizvod 3:50
12. Xue L, Islam MU, Koul AK, Wallace W, Bibby M (1997) Mater Manuf Process 12:799
13. Komvopoulos K, Nagarathnam K (1990) J Eng Mater Technol 112:131
14. Morisige N (1997) In: Khanna AS, Totlani MK, Singh SK (eds) Corrosion and it's control. Elsevier, Bombay
15. Ganamuthu DS (1980) Opt Eng 19:783
16. Jain AK, Kulkarni VK, Sood DK (1981) Appl Phys 25:127
17. Bergman HW, Mordike BL (1983) Z Werkstofftech 14:228
18. Kear BH, Breinan EM (1977) In: Proceedings of Sheffield international conference on solidification and casting, Sheffield
19. Singh J, Mazumder J (1986) Mater Sci Technol 2(7):709
20. Steen WM, Courtney CGH (1980) Met Technol June
21. Draper CW, Ewing CA (1984) J Mater Sci 19:3815
22. Draper CW, Poate JM (1985) J Int Met Rev 30:85
23. Jouvard JM, Grevey D, Lemoine F, Vannes AB (1997) J Phys (France) III 7:2265
24. Frenk A, Vandyoussefi M, Wagnière J-D, Zryd A, Kurz W (1997) Metall Mater Trans 28B:507
25. Li Y, Ma J (1997) Surf Coat Technol 90:1
26. Lin J (1996) J Laser Appl 12:28
27. Hayhurst P, Tuominen J, Mantyla J, Vuoristo P (2002) Proceedings of ICALEO 2002, Phoenix, AZ, October, LIA, paper 1201
28. Fellowes FC, Steen WM, Coley KS (1989) Proc. conf., IFHT, Lisbon, Portugal, September, p 435
29. Ayers JD, Schaefer RJ, Robey WP (1980) J Met Aug:19
30. Kloosterman AB, De Hosson JThM (1997) In: Aliabadi MH, Berbbia CA (eds) Surface treatment '97. Computational Mechanics Publications, Southampton, p 286
31. Hlawka F, Song GQ, Cornet A (1996) J Phys (France) IV Colloque C4 6:123
32. Hu C, Xin H, Baker TN (1995) J Mater Sci 30:5985
33. Ashby MF, Easterling KE (1984) Acta Metall 32:1935
34. Cline J, Anthony H (1977) J Appl Phys 48:3895
35. Davis M, Kapadia P, Dowden J, Steen WM, Courtney CHG (1986) J Phys D Appl Phys 19:1981
36. Bradley JR (1988) J Phys D Appl Phys 21:834
37. Das DK, Roy M, Singh AK, Sundararajan G (1996) Mater Sci Technol 12:295
38. Wang Y, Kovacevic R, Liu J (1998) Wear 221:47
39. Bharti A, Roy M, Sundararajan G (1992) In: Proceedings of 4th European conference on laser application, October, p 299
40. Staiaa MH, Cruza UM, Dahotre NB (2000) Thin Solid Films 377–378:665
41. Man HC, Zhang S, Cheng FT, Yue TM (2002) Scr Mater 46:229
42. Kwok CT, Cheng FT, Man HC (1998) Surf Coat Technol 107:31
43. Tassin C, Laroudie F, Pons M, Lelait L (1996) Surf Coat Technol 80:207
44. Fu Y, Batchelor AW (1998) Surf Coat Technol 102:119
45. Khedkar J, Khanna AS, Gupt KM (1997) Wear 205:220
46. Shamanian M, Mousavi Abarghouie SMR, Mousavi Pour SR (2010) Mater Des 31:2760
47. Grenier M, Dube D, Adnot A, Fishet M (1997) Wear 210:127

48. Guo B, Zhou J, Zhang S, Zhou H, Pu Y, Chen J (2008) Surf Coat Technol 202:4121
49. Staia MH, Cruz M, Dahotre NB (2001) Wear 251:1459
50. Dutta Majumdar J, Manna I (1999) Mater Sci Eng A268:227
51. Dutta Majumdar J, Manna I (1999) Mater Sci Eng A267:50
52. Dutta Majumdar J, Mordike BL, Manna I (2000) Wear 242:18
53. Manna I, Dutta Majumdar J, Ramesh Chandra B, Nayak S, Dahotre NB (2006) Surf Coat Technol 201:434
54. Persson DHE, Jacobson S, Hogmark S (2003) Wear 255:498
55. Jiang P, He XL, Li XX, Yu LG, Wang HM (2000) Surf Coat Technol 130:24
56. Hutchings IM (1992) Tribology. Edward Arnold, London
57. Rabinowicz E (1965) Friction and wear of materials. Wiley, New York
58. Lim SC, Ashby MF (1987) Acta Metall 35:11
59. Radek N, Bartkowiak K (2011) Phys Procedia 12:499
60. Quin TFJ, Sullivan JL, Rowson DM (1984) Wear 94:175
61. Rowson DM, Quinn TFJ (1980) J Phys D Appl Phys 13:209
62. Quin TFJ (1998) Wear 216:262–275
63. Malgaord J, Srivastaba VK (1977) Wear 41:263
64. Roy M, Ray KK, Sundararajan G (1999) Oxid Met 50
65. Hirose A, Ueda T, Kobayashi KF (1993) Mater Sci Eng 160A:143
66. Tau YH, Doong JL (1989) Wear 132:9
67. Isawane DT, Ma U (1989) Wear 129:123
68. Hou PY, Stringer J (1992) Oxid Met 38:323
69. Sigler DR (1993) Oxid Met 40:555
70. Bennett MJ, Haulton MR (1990) In: Bachelet E (ed) High temperature materials for power engineering. Kluwer Academic, Dordrecht, p 189
71. Tatlock GJ, Hard TJ (1984) Oxid Met 22:201
72. Gobel M, Rahmel A, Schertzc M (1993) Oxid Met 3–4:231
73. Sun JH, Jang HC, Chang E (1994) Surf Coat Technol 64:195
74. Vernon-Perry KD, Crovenor CRM, Needhan N, English T (1988) Mater Sci Technol 4:461
75. Pint BA (1997) Oxid Met 48:303
76. Ramnarayanan TA, Raghavan M, Petkvichuton R (1984) J Electrochem Soc 131:923
77. Forest C, Davidson JH (1995) Oxid Met 43:479
78. Walker A, Flower HM, West DRF (1985) J Mater Sci 20:989
79. Walker A, West DRF, Steen WM (1984) Mater Technol 11:399
80. Mordike BL, Bergmann HW, Grob N (1983) Z Werkstofftech 14:253
81. Shehata GH, Moussa AMA, Molian PA (1993) Wear 171:199
82. Nakata K, Tomoto K, Matsuda F (1996) Trans Jpn Weld Res Inst 25:37
83. Galun R, Weisheit A, Mordike BL (1996) J Laser Appl 8:299
84. Li R, Ferreira MJS, Anjos M, Vilar R (1996) Surf Coat Technol 88:90
85. Li R, Ferreira MJS, Anjos M, Vilar R (1996) Surf Coat Technol 88:96
86. Anjos M, Vilar R, Qui YY (1997) Surf Coat Technol 92:142
87. Belmondo A, Castagna M (1979) Thin Solid Films 64:249
88. Singh J, Majumder J (1987) Metall Trans 18:313
89. Folkes JA, Shibata K (1994) J Laser Appl 6:88
90. Roy A, Manna I (2001) Mater Sci Eng A297:85
91. Basu A, Chakraborty J, Shariff SM, Padmanabham G, Joshi SV, Sundararajan G, Dutta Majumdara J, Manna I (2007) Scr Mater 56:887
92. Padmavathi C, Sarin Sundar JK, Joshi SV, Prasad Rao K (2006) Trans Indian Inst Met 59:99
93. Staia MH, Cruz M, Dahotre NB (2000) Thin Solid Films 377–378:665
94. Ghosh K, McCay MH, Dahotre NB (1999) J Mater Process Technol 88:169
95. Rieker C, Morris DF, Steffen J (1989) Mater Sci Technol 5:590
96. Boas M, Bamberger M (1988) Wear 126:197
97. Sundararajan G, Schewmon PG (1983) Wear 84:237

98. Roy M, Das DK, Sivakumar R, Sundararajan G (1991) In: Darakadasa ES, Seshan S, Abraham KP (eds) Proceedings of the 2nd international conference on aluminium, July, Bangalore, p 947
99. Levy AV, Slamovich E, Jee N (1986) Wear 110:117
100. McIntyre M (1983) In: Metzbower EA (ed) Applications of lasers in material processing. ASM, Materials Park, OH
101. Regis V, Bracchetti M, Cerri W, Angelo DD, Mor GP (1990) In: Proceedings of high temperature materials for power engineering, September, Liege. Kluwer Academic, Dordrecht
102. Tanaka K, Saito T, Shimura Y, Mori K, Kawasaki M, Koyama M, Murase H (1993) J Jpn Inst Met 57:1114
103. Man HC, Cui ZD, Yue TM (2002) J Laser Appl 14:242
104. Lusquinos F, Pou J, Arias JL, Boutinguiza M, Leon B, Perez-Armor M (2001) In: Proceedings of ICALEO 2001, October, Jacksonville, FA, LIA, paper 1003
105. Liu Z, Watkins KG, Steen WM (1999) J Laser Appl 11:136
106. Liu Z, Pirch N, Gasser A, Watkins KG, Hatherley PG (2001) J Laser Appl 13:231
107. Anderson T (2002) Proceedings of ICALEO 2002, October, Pheonix, AZ, LIA, paper 1505
108. Padmavathi C, Sarin Sundar JK, Joshi SV, Prasad Rao K (2006) Mater Sci Technol 22:1
109. Zaplatynski I (1982) Thin Solid Film 95:275
110. Joshi SV, Sundararajan G (1998) In: Dahotre NB (ed) Lasers in surface engineering. ASM, Materials Park, OH, p 121
111. Pawlowski L (1999) J Therm Spray Technol 8(2):279
112. Voss A, Funken J, Alunovic M, Sung H, Kreutz EW (1992) Thin Solid Film 220:116
113. Funken J, Kreutz EW, Krische M, Sung H, Voss A, Erkens G, Lemmer O, Leyendeker T (1992) Surf Coat Technol 52:221
114. Oliveira JC, Paiva P, Oliveira MN, Conde O (1999) Appl Surf Sci 138–139:159
115. Wang Q, Schliesing R, Zacharias H, Buck V (1999) Appl Surf Sci 138–139:429
116. Zouari I, Lapicque F, Calvo M, Cabrera M (1990) Chem Eng Sci 45:2467
117. Grishko VI, Duley WW, Gu ZH, Fahidy TZ (2001) Electrochim Acta 47(4):643
118. Rebro PA, Shin YC, Incropera FP (2004) Int J Mach Tool Manuf 44(7–8):677
119. Ding H, Shin YC (2010) Int J Mach Tool Manuf 50(1):106
120. Bandyopadhyay S, Sarin Sundar JK, Sundararajan G, Joshi SV (2002) J Mater Process Technol 127:83
121. Tam SC, Willams R, Yang LJ, Jana S, Lim LEN, Lau MWS (1990) J Mater Process Technol 23:177
122. Pajak PT, De Silva AKM, McGough JA, Harrison DK (2004) J Mater Process Technol 149:512
123. Thomson G, Pridhan M (1998) Opt Laser Technol 30:191
124. Hoffmann E, Backes G, Gasser A, Kreutz EW, Stromeyer R, Wissenbach K (1996) Laser und Optoelektronik 28(3):59
125. Graydon O (1998) Opt Lasers Eng Feb:33